

LETTER

doi:10.1038/nature19339

Proteasome inhibition for treatment of leishmaniasis, Chagas disease and sleeping sickness

Shilpi Khare, Advait S. Nagle, Agnes Biggart, Yin H. Lai, Fang Liang, Lauren C. Davis, S. Whitney Barnes, Casey J. N. Mathison, Elmarie Myburgh, Mu-Yun Gao, J. Robert Gillespie, Xianzhong Liu, Jocelyn L. Tan, Monique Stinson, Ianne C. Rivera, Jaime Ballard, Vince Yeh, Todd Groessl, Glenn Federe, Hazel X. Y. Koh, John D. Venable, Badry Bursulaya, Michael Shapiro, Pranab K. Mishra, Glen Spraggan, Ansgar Brock, Jeremy C. Mottram, Frederick S. Buckner, Srinivasa P. S. Rao, Ben G. Wen, John R. Walker, Tove Tuntland, Valentina Molteni, Richard J. Glynne & Frantisek Supek

This is a PDF file of a peer-reviewed paper that has been accepted for publication. Although unedited, the content has been subjected to preliminary formatting. *Nature* is providing this early version of the typeset paper as a service to our customers. The text and figures will undergo copyediting and a proof review before the paper is published in its final form. Please note that during the production process errors may be discovered which could affect the content, and all legal disclaimers apply.

Cite this article as: Khare, S. et al. Proteasome inhibition for treatment of leishmaniasis, Chagas disease and sleeping sickness. *Nature* http://dx.doi.org/10.1038/nature19339 (2016).

Competing financial interests statement: Patents related to this work have been filed (WO 2015/095477 A1, WO 2014/151784 A1, WO 2014/151729). Several authors own shares of Novartis.

Received 23 December 2015; accepted 1 August 2016.

Accelerated Article Preview Published online 8 August 2016.

Proteasome inhibition for treatment of leishmaniasis, Chagas disease and sleeping sickness

Shilpi Khare^{1*}, Advait S. Nagle^{1*}, Agnes Biggart¹, Yin H. Lai¹, Fang Liang¹, Lauren C. Davis¹, S. Whitney Barnes¹, Casey J. N. Mathison¹, Elmarie Myburgh^{2,3}, Mu-Yun Gao¹, J. Robert Gillespie⁴, Xianzhong Liu¹, Jocelyn L. Tan¹, Monique Stinson¹, Ianne C. Rivera¹, Jaime Ballard¹, Vince Yeh¹, Todd Groessl¹, Glenn Federe¹, Hazel X. Y. Koh⁵, John D. Venable¹, Badry Bursulaya¹, Michael Shapiro¹, Pranab K. Mishra¹, Glen Spraggan¹, Ansgar Brock¹, Jeremy C. Mottram^{2,3}, Frederick S. Buckner⁴, Srinivasa P. S. Rao⁵, Ben G. Wen¹, John R. Walker¹, Tove Tuntland¹, Valentina Molteni¹, Richard J. Glynn¹ & Frantisek Supek¹

Chagas disease, leishmaniasis and sleeping sickness affect 20 million people worldwide and lead to more than 50,000 deaths annually¹. The diseases are caused by infection with the kinetoplastid parasites *Trypanosoma cruzi*, *Leishmania* spp. and *Trypanosoma brucei* spp., respectively. These parasites have similar biology and genomic sequence, suggesting that all three diseases could be cured with drug(s) modulating the activity of a conserved parasite target². However, no such molecular targets or broad spectrum drugs have been identified to date. Here we describe a selective inhibitor of the kinetoplastid proteasome (GNF6702) with unprecedented *in vivo* efficacy, which cleared parasites from mice in all three models of infection. GNF6702 inhibits the kinetoplastid proteasome through a non-competitive mechanism, does not inhibit the mammalian proteasome or growth of mammalian cells, and is well-tolerated in mice. Our data provide genetic and chemical validation of the parasite proteasome as a promising therapeutic target for treatment of kinetoplastid infections, and underscore the possibility of developing a single class of drugs for these neglected diseases.

Kinetoplastid infections affect predominantly poor communities in Latin America, Asia and Africa. Available therapies suffer from multiple shortcomings, and new drug discovery for these diseases is limited by insufficient investment³. We sought low molecular weight compounds with a growth inhibitory effect on *Leishmania donovani* (*L. donovani*)^{4,5}, *Trypanosoma cruzi* (*T. cruzi*)^{6,7} and *Trypanosoma brucei* (*T. brucei*)^{5,8}. Our approach was to test 3 million compounds in proliferation assays on all three parasites (Supplementary Information Tables 1–3), followed by triaging of active compounds (half-maximum inhibitory concentration value EC₅₀<10 μM) to select those with a clear window of selectivity (>5-fold) with respect to growth inhibition of mammalian cells. An azabenzoxazole, GNF5343, was identified as a hit in the *L. donovani* and *T. brucei* screens. Although GNF5343 was not identified in the *T. cruzi* screen, we noted potent anti-*T. cruzi* activity of this compound in secondary assays.

Optimization of GNF5343 involved the design and synthesis of ~3,000 compounds, and focused on improving bioavailability and potency on inhibition of *L. donovani* growth within macrophages (Fig. 1). A critical modification involved replacement of the azabenzoxazole center with C6-substituted imidazo- and triazolopyrimidine cores, which yielded compounds up to 20-fold more potent on intra-macrophage *L. donovani* (e.g. GNF2636). Replacement of the furan group with a dimethyloxazole ring reduced the risk of toxicity associated with the furan moiety, and replacement of the chlorophenyl group with a fluorophenyl improved selectivity over mammalian cell growth inhibition (e.g. GNF3849). These changes also resulted in low clearance and acceptable bioavailability. Further substitutions at the core C6 position

led to GNF6702 and a 400-fold increase in intra-macrophage *L. donovani* potency compared to GNF5343.

L. donovani parasites cause a majority of visceral leishmaniasis (VL) cases in East Africa and India⁹. In mice infected with *L. donovani*¹⁰, oral dosing with GNF6702 effected a more pronounced reduction in liver parasite burden than miltefosine, the only oral anti-leishmanial drug available in clinical practice⁵ (Fig. 2a). The miltefosine regimen for VL efficacy studies was chosen to approximate the drug plasma concentration of the clinical regimen¹¹. We noted a greater than three log reduction in parasite load after eight day treatment with 10 mg/kg of GNF6702 twice-daily with the free concentration of GNF6702 (fraction unbound in plasma = 0.063) staying above the *L. donovani* EC₉₉ value (the concentration inhibiting 99% of intra-macrophage parasite growth *in vitro*) for the duration of the dosing period (Extended Data Fig. 1a). Characterization of efficacy of ten analogues in the series at various doses revealed a significant correlation ($r^2 = 0.89$, p<0.01) between i) the ratio of mean free plasma compound concentration to the *L. donovani* EC₉₀ value and ii) reduction of the liver parasite burden. We found that 90% parasite burden reduction in the mouse model was achieved when the mean free compound plasma concentration during treatment equaled a 0.94-fold multiple of the *L. donovani* EC₉₀ value (Fig. 2b).

Cutaneous leishmaniasis (CL) affects about a million people per year, causing skin lesions that can resolve into scar tissue¹². In parts of the Middle East, CL has reached epidemic proportions¹³. After footpad infection of BALB/c mice with the dermatotropic *L. major* strain^{14,15}, treatment with GNF6702 at 10 mg/kg twice-daily caused a 5-fold decrease in footpad parasite burden and a reduction in footpad swelling (Fig. 2c). Both 3 mg/kg and 10 mg/kg twice-daily regimens of GNF6702 were superior to 30 mg/kg once-daily miltefosine regimen (p<0.01), which translates into ~2-fold higher miltefosine plasma concentration in mice than observed in clinical dosing¹¹.

We further tested if GNF6702 can cure additional kinetoplastid parasite infections. An estimated 25% of the 8 million people infected with *T. cruzi* will develop chronic Chagas disease, manifesting as cardiac or intestinal dysfunction^{16,17}. Benznidazole is broadly used for treatment of acute and indeterminate stages of Chagas disease in Latin America^{18,19}. However, benznidazole has side-effects that frequently lead to treatment interruption^{18,20–22} and a better tolerated drug is needed. To model treatment in the indeterminate disease stage, we infected mice with *T. cruzi* parasites and began treatment 35 days after infection, when the immune system of the mice had controlled parasite burden²³. We increased the parasite detection sensitivity by immunosuppressing the mice after 20 days of treatment^{23,24}. In this model, GNF6702 dosed twice-daily at 10 mg/kg matched the efficacy of benznidazole at 100 mg/kg once-daily; all but one treated mice had no

¹Genomics Institute of the Novartis Research Foundation, San Diego, California 92121, USA. ²Wellcome Trust Centre for Molecular Parasitology, Institute of Infection, Immunity and Inflammation, College of Medical, Veterinary and Life Sciences, University of Glasgow, Glasgow G12 8TA, UK. ³Centre for Immunology and Infection, Department of Biology, University of York, Wentworth Way, Heslington, York, YO10 5DD, UK. ⁴Department of Medicine, University of Washington, Seattle, Washington 98109, USA. ⁵Novartis Institute for Tropical Diseases, Singapore.

*These authors contributed equally to this work.

detectable parasites in blood, colon or heart tissue, even after 4 weeks of immunosuppression (Fig. 2d).

Finally, we tested GNF6702 in a mouse model of stage II sleeping sickness (human African trypanosomiasis - HAT)²⁵. Mortality of stage II HAT is caused by infection of the CNS and, in this mouse model, luciferase-expressing *T. brucei* parasites establish a CNS infection by day 21 post-infection. GNF6702 was administered at 100 mg/kg once-daily to account for low exposure in the brain relative to the plasma (~10%, Extended Data Fig. 1b). Diminazene acetate, a stage I drug that poorly crosses the blood-brain barrier, effected apparent clearance of parasites from the blood after a single dose, but did not prevent parasite recrudescence 21 days later. By contrast, treatment with GNF6702 for seven days caused a sustained clearance of parasites (days 42 and 92 post-infection in Fig. 2e, Extended Data Fig. 2a, Supplementary Information Tables 4 and 5). Significantly, mice treated with GNF6702 had no detectable parasites in the brain at termination of the experiment, though parasites were clearly detected in the brains of mice treated with diminazene acetate (Extended Data Fig. 2b, Supplementary Information Table 6).

As GNF6702 showed compelling efficacy in four mouse models of kinetoplastid infections: VL, CL, Chagas disease and stage II HAT, we reasoned that mechanistic studies of GNF6702 might identify a pan-kinetoplastid drug target that could inform target-based drug discovery efforts. We attempted to evolve *L. donovani* strains resistant to GNF3943 and GNF8000 (early analogues from the series, Extended Data Fig. 3) through 12 months of parasite culture under drug pressure without success. However, we were able to select two drug-resistant *T. cruzi* epimastigote isolates, one resistant to GNF3943, and another to GNF8000. Both *T. cruzi* lines exhibited at least 40-fold lower susceptibility to GNF6702 than wild type *T. cruzi* (Extended Data Fig. 4a and 4b). Using whole genome sequencing, we found that the GNF3943-resistant line had a homozygous mutation encoding a substitution of isoleucine for methionine at amino acid 29 in the proteasome beta 4 subunit (*PSMB4^{I29M/I29M}*) and a heterozygous mutation P82L in dynein heavy chain gene. The GNF8000-resistant line had a heterozygous F24L mutation in *PSMB4*, and four other heterozygous mutations (Extended Data Table 1). We focused our attention on the proteasome as a likely target for the compound series because we found two independent mutations in the *PSMB4* gene, and because the proteasome is an essential enzyme in eukaryotic cells. We also note that the *Plasmodium falciparum* proteasome has recently been the target of promising drug discovery efforts for malaria²⁶.

We first asked whether two prototypic inhibitors of mammalian proteasome, bortezomib and MG132, could also block *T. cruzi* growth. Indeed, both compounds inhibited *T. cruzi* epimastigote proliferation with sub-micromolar potency. However, in contrast to GNF6702, bortezomib and MG132 inhibited proliferation of the two resistant lines (*PSMB4^{I29M/I29M}*, *PSMB4^{WT/F24L}*) with comparable potency to the wild type parasites. Additionally, the *PSMB4* mutant lines were not resistant to nifurtimox, an anti-kinetoplastid drug with an unrelated mechanism of action (Extended Data Fig. 4a and 4b). To determine whether the F24L mutation was sufficient to confer resistance to GNF6702, we engineered *T. cruzi* epimastigote lines that ectopically expressed either wild type or F24L-mutated PSMB4. Overexpression of *PSMB4^{WT}* had little effect on the EC₅₀ value for GNF6702, whereas overexpression of *PSMB4^{F24L}* caused a greater than 10-fold reduction in GNF6702 potency, but not in that of bortezomib (Fig. 3a, Extended Data Fig. 4c). Previously, bortezomib was also shown to inhibit the growth of *T. brucei*, suggesting that proteasome activity is essential for growth in this parasite as well²⁷. To test whether *PSMB4^{F24L}* can rescue growth inhibition by GNF6702 in *T. brucei*, we engineered two parasite strains that ectopically expressed wild type and F24L-mutated PSMB4, respectively. Similar to *T. cruzi*, overexpression of *PSMB4^{F24L}* in *T. brucei* conferred a high level of resistance to GNF6702 (~70-fold shift in EC₅₀ value), while having no effect on parasite susceptibility to bortezomib (Fig. 3b, Extended Data Fig. 4c).

We next asked whether GNF6702 could inhibit any of three *T. cruzi* proteasome proteolytic activities in biochemical assays. As predicted from the *T. cruzi* genome²⁸, mass spectrometry analysis of purified *T. cruzi* proteasome identified seven alpha and seven beta proteasome subunits, including PSMB4 (Supplementary Tables 7 and 8). Using substrates that are specific for each of the chymotrypsin-like, trypsin-like and caspase-like proteolytic activities, we found that only the chymotrypsin-like activity of the *T. cruzi* proteasome was inhibited by GNF6702 (IC₅₀ = 35 nM), while the other two activities were not affected (IC₅₀>10 μM). In contrast, bortezomib inhibited the chymotrypsin-like (IC₅₀ = 91 nM), the caspase-like (IC₅₀ = 370 nM) and the trypsin-like (IC₅₀ = 1.7 μM) activities. We further found that the chymotrypsin-like activity of the PSMB4^{I29M} *T. cruzi* proteasome was at least 300-fold less susceptible to GNF6702 (IC₅₀>10 μM) and ~3-fold less susceptible to bortezomib (IC₅₀ = 0.26 μM), while susceptibility of the other two mutant proteasome proteolytic activities to the two inhibitors were not affected (Fig. 4a, Extended Data Table 2).

We reasoned that if the primary mechanism of parasite growth inhibition by the compound series was through inhibition of the proteasome chymotrypsin-like activity, then the IC₅₀ values for this proteolytic activity should correlate with EC₅₀ values for parasite proliferation. Indeed, a tight correlation between the two parameters was observed for *L. donovani* axenic amastigotes and *T. brucei* bloodstream form trypomastigotes ($r^2 = 0.78$ and $r^2 = 0.67$, respectively) over a 2,000-fold potency range for 317 analogues, thus indicating that inhibition of parasite proteasome activity was driving the anti-parasitic activity of these compounds. We observed a weaker correlation between IC₅₀ and EC₅₀ values for intracellular *T. cruzi* ($r^2 = 0.36$, $p < 0.01$), perhaps reflecting more complex cellular pharmacokinetics resulting from compounds having to access *T. cruzi* parasites within the cytosol of mammalian cells (Fig. 4b, Extended Data Fig. 5).

Both resistant *T. cruzi* lines retained sensitivity to bortezomib, which is a substrate-competitive inhibitor, suggesting that GNF6702 might have an alternative mode of inhibition. A Lineweaver-Burk plot of chymotrypsin-like activity at increasing concentrations of peptide substrate showed that GNF6702 has a non-competitive mode of inhibition clearly distinct from the competitive mechanism described for MG132 and bortezomib^{29,30}. We were also able to extend these observations to proteasome from *L. donovani* (Fig. 4c, Extended Data Table 3). We further note that GNF6702 had no measurable activity on the human proteasome (Fig. 4d, Extended Data Table 2). Interestingly, human proteasome beta 4 subunit has a methionine at the 29th amino acid position, mirroring the I29M mutation in the GNF3943-resistant *T. cruzi* line (Extended Data Fig. 6a).

In summary, GNF6702 blocks the chymotrypsin-like activity harbored by the beta 5 subunit without competing with substrate binding, and mutations in the beta 4 subunit, which is in direct physical contact with the beta 5 subunit, confer resistance to this inhibition. Next we used homology modeling of the *T. cruzi* proteasome to look for evidence of an allosteric inhibitor binding site. In the *T. cruzi* proteasome model, the F24 and I29 beta 4 residues are positioned at the interface between the beta 4 and beta 5 subunits, on the outer limit of the beta 5 active site. Adjacent to these two beta 4 residues and the beta 5 active site is a plausible binding pocket for GNF6702 (Extended Data Fig. 6b and 6c).

Finally, we tested whether GNF6702 can inhibit proteasome activity in intact *T. cruzi* cells. Cellular proteins entering the proteasome degradation pathway are first tagged with ubiquitin, and proteasome inhibition results in intracellular accumulation of ubiquitylated proteins. Treatment of *T. cruzi* epimastigotes with GNF6702 led to significant buildup of ubiquitylated proteins (Extended Data Fig. 7a) with the half-maximal effect (EC₅₀) achieved at 130 nM compound concentration (Extended Data Fig. 7c). This EC₅₀ value correlated well with the half-maximal growth inhibitory concentration of GNF6702 on *T. cruzi* epimastigotes (EC₅₀ = 150 nM; Extended Data Fig. 4b).

For comparison, similar experiments with bortezomib yielded comparable inhibitor potencies in the two *T. cruzi* assays (ubiquitylation EC₅₀ = 62 nM vs growth inhibition EC₅₀ = 160 nM; Extended Data Fig. 4b and 7c). We did not observe any detectable accumulation of ubiquitylated proteins in mammalian 3T3 cells treated with GNF6702 (Extended Data Fig. 7b and 7c), further confirming high selectivity of this compound.

Validation of the parasite proteasome as the target of GNF6702 is supported through several lines of evidence: i) point mutations in the *PSMB4* gene are sufficient to confer resistance to biochemical proteasome inhibition and cellular *T. cruzi* growth inhibition; ii) GNF6702 is a selective inhibitor of parasite proteasome activity and does not inhibit the human proteasome, mirroring the selective inhibition of parasite growth over mammalian cell growth; and iii) potency of GNF6702 and analogues in parasite proteasome assays predict potency in parasite growth inhibition assays.

In this work we show that in mouse disease models, GNF6702 was able to eradicate parasites from diverse niches that included the cytosol (*T. cruzi*), phagolysosome (*L. donovani*, *L. major*) of infected host cells, and brain (*T. brucei*). GNF6702 has also good pharmacokinetic properties, and the compound did not show activity in panels of human receptor, enzyme and ion channel assays (Supplementary Tables 9–11). Going forward, GNF6702, or analogues thereof, has potential to yield a new treatment for several kinetoplastid infections and it is currently being evaluated in preclinical toxicity studies. It is unclear if the clinical utility of GNF6702 could extend to the treatment of stage II HAT as GNF6702 was tested in the HAT mouse model only at one high dose (100 mg/kg once-daily). We also note that identification of a broadly active pan-kinetoplastid drug might not be feasible (or desirable) as such a drug would need to reach high concentrations in varied tissues/subcellular compartments, and might carry increased toxicity risk. Instead, alternative analogues from this series with different pharmacological profiles might be needed for treatment of different kinetoplastid infections. Nevertheless, there are only scarce resources for drug development in these diseases, and identification of a common target and chemical scaffold with potential across multiple indications provides new hope for improved treatment options for some of the world's poorest people.

Online Content Methods, along with any additional Extended Data display items and Source Data, are available in the online version of the paper; references unique to these sections appear only in the online paper.

Received 23 December 2015; accepted 1 August 2016.

Published online 8 August 2016.

- Research priorities for Chagas disease, human African trypanosomiasis and leishmaniasis. *World Health Organization, WHO Technical Report Series* **975**, 1–100 (2012).
- El-Sayed, N. M. et al. Comparative genomics of trypanosomatid parasitic protozoa. *Science* **309**, 404–409, doi:10.1126/science.1112181 (2005).
- Bilbe, G. Infectious diseases. Overcoming neglect of kinetoplastid diseases. *Science* **348**, 974–976, doi:10.1126/science.aaa3683 (2015).
- Sundar, S. & Chakravarty, J. An update on pharmacotherapy for leishmaniasis. *Expert Opinion on Pharmacotherapy* **16**, 237–252, doi:10.1517/14656566.2015.973850 (2015).
- Nagle, A. S. et al. Recent developments in drug discovery for leishmaniasis and human African trypanosomiasis. *Chemical Reviews*, doi:10.1021/cr500365f (2014).
- Bern, C. Chagas' Disease. *The New England Journal of Medicine* **373**, 456–466, doi:10.1056/NEJMra1410150 (2015).
- Chatelain, E. Chagas disease drug discovery: toward a new era. *Journal of Biomolecular Screening* **20**, 22–35, doi:10.1177/1087057114550585 (2015).
- Kennedy, P. G. Clinical features, diagnosis, and treatment of human African trypanosomiasis (sleeping sickness). *The Lancet. Neurology* **12**, 186–194, doi:10.1016/S1474-4422(12)70296-X (2013).
- Control of the leishmaniasis. *World Health Organization, WHO Technical Report Series* **949**, 37–39 (2010).
- Yardley, V. & Croft, S. L. A comparison of the activities of three amphotericin B lipid formulations against experimental visceral and cutaneous leishmaniasis. *International Journal of Antimicrobial Agents* **13**, 243–248 (2000).

- Dorlo, T. P. et al. Pharmacokinetics of miltefosine in Old World cutaneous leishmaniasis patients. *Antimicrobial Agents and Chemotherapy* **52**, 2855–2860, doi:10.1128/AAC.00014-08 (2008).
- McGwire, B. S. & Satoskar, A. R. Leishmaniasis: clinical syndromes and treatment. *QJM : Monthly journal of the Association of Physicians* **107**, 7–14, doi:10.1093/qjmed/hct116 (2014).
- Hotez, P. J. Combating the next lethal epidemic. *Science* **348**, 296–297, doi:10.1126/science.348.6232.296-b (2015).
- Sacks, D. & Anderson, C. Re-examination of the immunosuppressive mechanisms mediating non-cure of *Leishmania* infection in mice. *Immunological Reviews* **201**, 225–238, doi:10.1111/j.0105-2896.2004.00185.x (2004).
- Nelson, K. G., Bishop, J. V., Ryan, R. O. & Titus, R. Nanodisk-associated amphotericin B clears *Leishmania major* cutaneous infection in susceptible BALB/c mice. *Antimicrobial Agents and Chemotherapy* **50**, 1238–1244, doi:10.1128/AAC.50.4.1238-1244.2006 (2006).
- Nunes, M. C. et al. Chagas disease: an overview of clinical and epidemiological aspects. *Journal of the American College of Cardiology* **62**, 767–776, doi:10.1016/j.jacc.2013.05.046 (2013).
- Coura, J. R. & Borges-Pereira, J. Chagas disease: 100 years after its discovery. A systemic review. *Acta Tropica* **115**, 5–13, doi:10.1016/j.actatropica.2010.03.008 (2010).
- Bern, C. Antitrypanosomal therapy for chronic Chagas' disease. *The New England Journal of Medicine* **364**, 2527–2534, doi:10.1056/NEJMct1014204 (2011).
- Viotti, R. et al. Towards a paradigm shift in the treatment of chronic Chagas disease. *Antimicrobial Agents and Chemotherapy* **58**, 635–639, doi:10.1128/AAC.01662-13 (2014).
- Molina, I. et al. Randomized trial of posaconazole and benznidazole for chronic Chagas' disease. *The New England Journal of Medicine* **370**, 1899–1908, doi:10.1056/NEJMoa1313122 (2014).
- Morillo, C. A. et al. Randomized trial of benznidazole for chronic Chagas' cardiomyopathy. *The New England Journal of Medicine* **373**, 1295–1306, doi:10.1056/NEJMoa1507574 (2015).
- Viotti, R. et al. Side effects of benznidazole as treatment in chronic Chagas disease: fears and realities. *Expert Review of Anti-Infective Therapy* **7**, 157–163, doi:10.1586/14787210.7.2.157 (2009).
- Khare, S. et al. Antitrypanosomal treatment with benznidazole is superior to posaconazole regimens in mouse models of Chagas disease. *Antimicrobial Agents and Chemotherapy* **59**, 6385–6394, doi:10.1128/AAC.00689-15 (2015).
- Bustamante, J. M., Bixby, L. M. & Tarleton, R. L. Drug-induced cure drives conversion to a stable and protective CD8+ T central memory response in chronic Chagas disease. *Nature Medicine* **14**, 542–550, doi:10.1038/nm1744 (2008).
- Myburgh, E. et al. In vivo imaging of trypanosome-brain interactions and development of a rapid screening test for drugs against CNS stage trypanosomiasis. *PLoS Neglected Tropical Diseases* **7**, e2384, doi:10.1371/journal.pntd.0002384 (2013).
- Li, H. et al. Structure- and function-based design of *Plasmodium*-selective proteasome inhibitors. *Nature* **530**, 233–236, doi:10.1038/nature16936 (2016).
- Steverding, D. & Wang, X. Trypanocidal activity of the proteasome inhibitor and anti-cancer drug bortezomib. *Parasites & Vectors* **2**, 29, doi:10.1186/1756-3305-2-29 (2009).
- Ivens, A. C. et al. The genome of the kinetoplastid parasite, *Leishmania major*. *Science* **309**, 436–442, doi:10.1126/science.1112680 (2005).
- Li, X. et al. Effect of noncompetitive proteasome inhibition on bortezomib resistance. *Journal of the National Cancer Institute* **102**, 1069–1082, doi:10.1093/jnci/djq198 (2010).
- Fernandez, Y. et al. Chemical blockage of the proteasome inhibitory function of bortezomib: impact on tumor cell death. *The Journal of Biological Chemistry* **281**, 1107–1118, doi:10.1074/jbc.M511607200 (2006).

Supplementary Information is available in the online version of the paper.

Acknowledgements This work was supported in part by grants from the Wellcome Trust (091038/Z/09/Z to R.J.G. and F.S., and 104976/Z/14/Z, 104111/15/Z to J.C.M. and E.M.) and NIH (AI106850 to F.S.B.). We thank Simon Croft, Rob Don, Lars Gredsted, Alan Hudson and John Mendlein for discussions, Rick Tarleton for *T. cruzi* CL strain, and George Cross for *T. brucei* Lister 427 strain. We thank Andreas Kreusch for help with proteasome purification, and Fabio Luna for help with *T. cruzi* whole genome sequencing. We acknowledge technical assistance of Ormeed Faghini in generating the plasmids for ectopic expression of *PSMB4* in *T. cruzi*, Ryan Ritchie for IVIS *in vivo* imaging, and Annie Mak, Jason Matzen and Paul Anderson for execution of high throughput screens. We thank John Isbell and Thomas Hollenbeck for profiling GNF6702 in ADME assays.

Author Contributions A.B., F.L., C.J.N.M., P.K.M., A.S.N., J.L.T. and V.Y. designed chemical analogues, and performed chemical synthesis and purification of synthesized analogues. F.S.B., J.B., J.R.G., S.K., H.X.Y.K., Y.H.L., S.P.S.R., F.S., and X.L. conducted and analyzed data from *in vitro* growth inhibition assays. L.C.D., X.L., J.C.M., E.M., I.C.R., S.P.S.R., M.S., F.S., and B.G.W. conducted and analyzed data from *in vivo* efficacy assays. J.B., M.-Y.G., S.K., and F.S. conducted proteasome purification, proteasome inhibition assays and biochemical data

analysis. S.W.B., G.F., S.K., F.S., and J.R.W. designed, conducted and analyzed experiments resulting in identification of proteasome resistance mutations. G.S. and B.B. built the homology model of *T. cruzi* proteasome structure and performed GNF6702 docking. A.B. and J.D.V. analyzed *T. cruzi* proteasome by mass spectrometry. A.N., T.G., M.S., F.S., and T.T. designed, conducted, and analyzed PK data. A.N. and V.M. led the chemistry team. F.S. led the biology team. R.J.G. and F.S. supervised and led the overall project, and led the writing of the manuscript. All authors contributed to writing of the manuscript.

Author Information Reprints and permissions information is available at www.nature.com/reprints. The authors declare competing financial interests: details are available in the online version of the paper. Readers are welcome to comment on the online version of the paper. Correspondence and requests for materials should be addressed to F.S. (fsupek@gnf.org).

Reviewer Information *Nature* thanks M. Philips, S. Schreiber and the other anonymous reviewer(s) for their contribution to the peer review of this work.

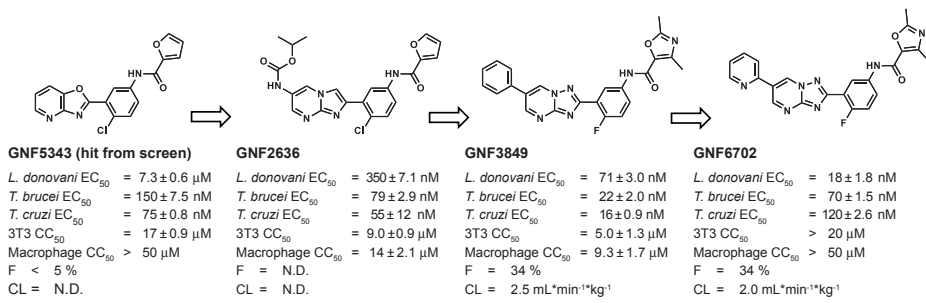


Figure 1 | Chemical evolution of GNF6702 from the phenotypic hit GNF5343. *L. donovani*: amastigotes proliferating within primary mouse macrophages; *T. brucei*: the bloodstream form trypomastigotes; *T. cruzi*: amastigotes proliferating in 3T3 fibroblast cells; macrophage: mouse primary peritoneal macrophages; EC₅₀ and CC₅₀: half-maximum

growth inhibition concentration; F: oral bioavailability in mouse after administering single compound dose (20 mg/kg) as a suspension; CL: plasma clearance in mouse after single iv bolus dose (5 mg/kg); N.D.: not determined; all EC₅₀ and CC₅₀ values correspond to means ± s.e.m. (n = 4 technical replicates).

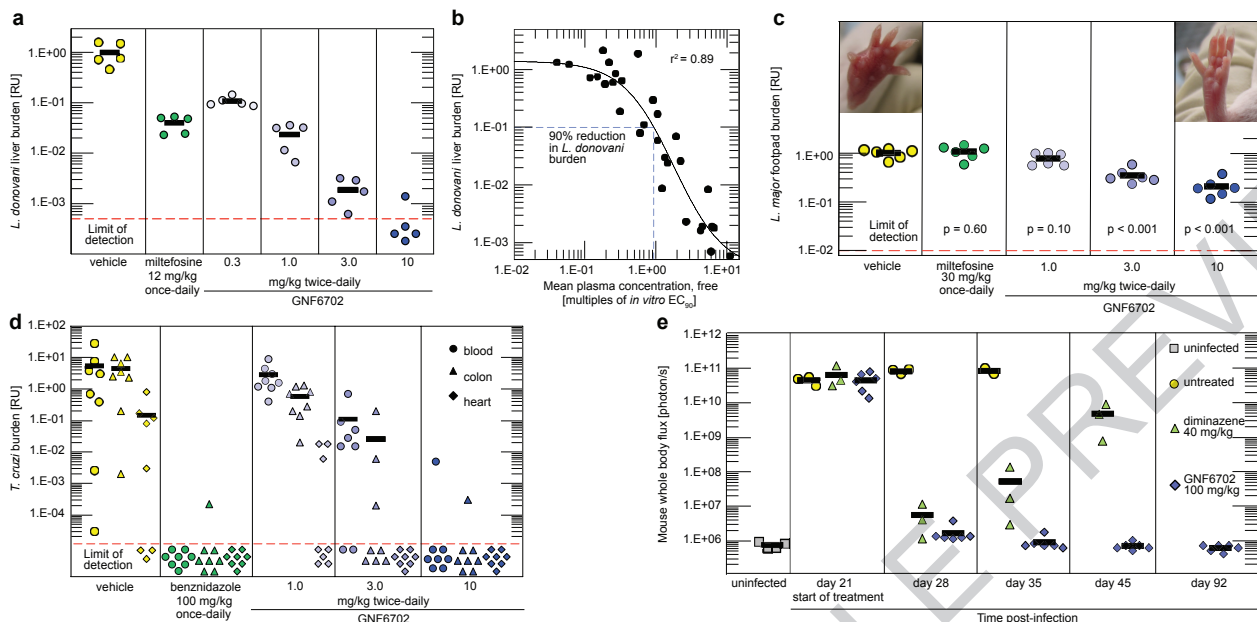


Figure 2 | GNF6702 clears parasites in mouse models of kinetoplastid infections. **a**, Post-treatment *L. donovani* liver burdens in mouse model of VL as assessed by qPCR ($n = 5$ mice). **b**, PK/PD relationship for ten GNF6702 analogues, each administered at several doses; circles: mean liver burdens associated with individual compound regimens (30 regimens in total; $n = 5$ mice per regimen) relative to vehicle; horizontal dotted line: 90% reduction in the liver *L. donovani* burden; vertical dotted line: 0.94-fold multiple of the mean free compound plasma concentration/the *L. donovani* EC₉₀ value ratio. **c**, Post-treatment *L. major* footpad burdens in the BALB/c mouse model of CL as assessed by qPCR ($n = 6$ mice); the *p* values (two-tailed distribution) relate parasite burdens in compound-treated mice with those from vehicle-treated mice; left inset picture: a representative mouse footpad after treatment with vehicle; right inset picture: a representative mouse footpad after treatment with GNF6702 10 mg/kg twice-daily regimen. **d**, *T. cruzi* burden in mouse blood (circles), colon (triangles) and heart (diamonds) as assessed by qPCR after 20 days of treatment and four weeks of immunosuppression ($n = 8$ mice).

e, Whole body *in vivo* imaging of bioluminescent *T. brucei* before and after treatment; *Trypanosoma brucei*-infected mice were treated by a single intraperitoneal injection of diminazene aceturate ($n = 3$ mice) or by oral administration of GNF6702 once-daily for 7 days ($n = 6$ mice); filled symbols show whole body bioluminescence values for individual mice; several mice from the untreated and diminazene aceturate-treated groups were euthanized between days 28 and 56 due to CNS infection symptoms; background bioluminescence values shown for uninfected mice (grey-filled squares; $n = 4$) were collected independently from mice aged-matched for day 0 using the same acquisition settings. Red dotted lines in **a**, **c** and **d** plots show limit of parasite detection by qPCR; plot symbols below the red dotted line: mice with no detectable parasites; data points below the limit of detection are ‘jittered’ to show number of animals in a group; thick horizontal lines: means of the treatment groups; RU: relative units (parasite burden relative to the mean burden of the vehicle-treated group).

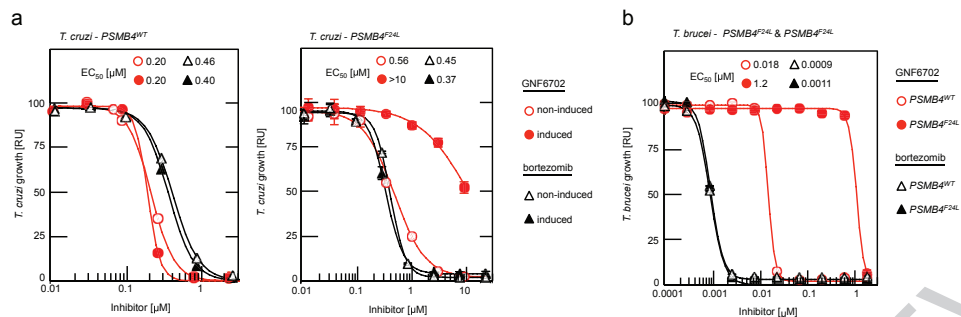


Figure 3 | F24L mutation in proteasome beta 4 subunit confers selective resistance to GNF6702. **a**, growth inhibition of *T. cruzi* epimastigote strains ectopically expressing PSMB4^{WT} or PSMB4^{F24L} protein by GNF6702 and bortezomib; non-induced/induced: culture medium without/with tetracycline to modulate expression of tetracycline-inducible PSMB4 genes. **b**, growth inhibition of *T. brucei* bloodstream form trypanosomes constitutively overexpressing PSMB4^{WT} or PSMB4^{F24L} protein by GNF6702 and bortezomib. EC₅₀ values for each strain/

compound pair are listed inside **a** and **b** plot panels next to corresponding strain/compound symbol (defined in plot legends); means from n = 3 technical replicates are shown; error bars represent s.e.m. values; for data points lacking error bars, s.e.m. values are smaller than circles representing means; due to limited aqueous solubility, the highest tested GNF6702 concentration was 10 μ M. RU (relative units) in **a** and **b** corresponds to parasite growth relative to the DMSO control (%).

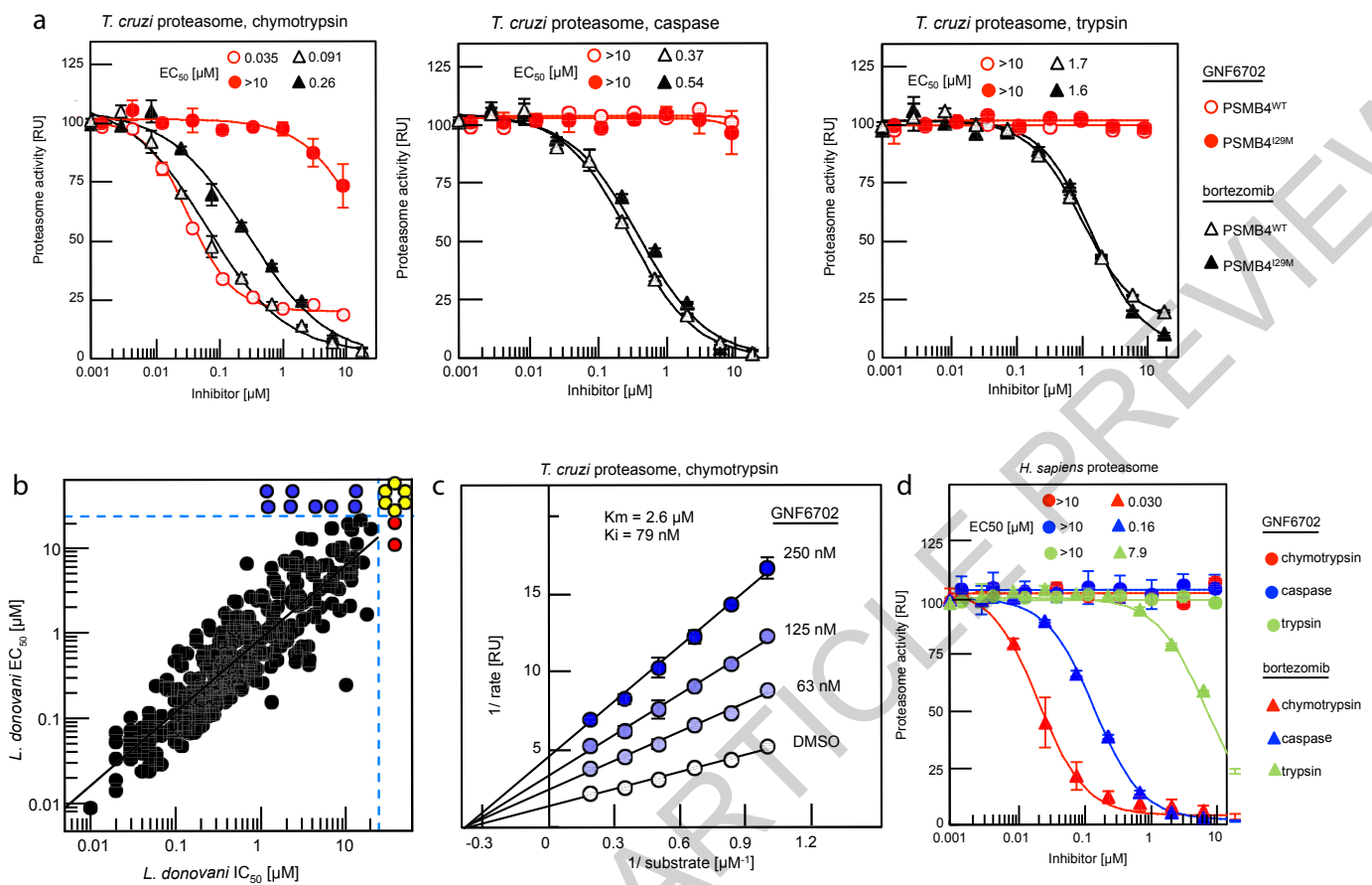


Figure 4 | Compounds from GNF6702 series inhibit growth of kinetoplastid parasites by inhibiting parasite proteasome chymotrypsin-like activity. **a**, Inhibition of three proteolytic activities of purified wild type (PSMB4^{WT}) and PSMB4^{129M} *T. cruzi* proteasomes by GNF6702 and bortezomib; IC₅₀ values for proteasome proteolytic activities are listed inside plots. **b**, Correlation between inhibition of chymotrypsin-like activity of purified *L. donovani* proteasome (IC₅₀) and *L. donovani* axenic amastigote growth inhibition (EC₅₀; data points correspond to means of 2 technical replicates); red circles: IC₅₀>20 μM; blue circles: EC₅₀>25 μM; yellow circles: IC₅₀>20 μM and EC₅₀>25 μM;

data for 317 analogues are shown. **c**, Lineweaver-Burk plot of inhibition of *T. cruzi* proteasome chymotrypsin-like activity by GNF6702 at increasing concentrations of a peptide substrate. **d**, Effect of GNF6702 and bortezomib on three proteolytic activities of human constitutive proteasome; IC₅₀ values for proteasome proteolytic activities are listed inside plots. Data shown in **a**, **c** and **d** represent means \pm s.e.m. ($n = 3$ technical replicates; for data points lacking error bars, s.e.m. values are smaller than circles representing means). Due to limited aqueous solubility, the highest tested GNF6702 concentration in experiments shown in **a** and **d** was 10 μ M.

METHODS

Ethics statement for animal models. All procedures involving mice were performed in accordance with AAALAC standards or under UK Home Office regulations, and were reviewed and approved in accordance with the Novartis Animal Welfare Policy. Sample size was determined on the basis of the minimum number of animals required for good data distribution and statistics. Blinding was not possible in these experiments but animals were selected randomly for each group. **Determination of IC₅₀, EC₅₀, and CC₅₀ values.** Reported IC₅₀/ EC₅₀/ CC₅₀ values were calculated by averaging IC₅₀/ EC₅₀/ CC₅₀ values obtained from individual technical replicate experiments (n; specified in relevant Figure captions and Methods sub-sections). Each technical replicate experiment was performed on a different day with freshly prepared reagents. Reported standard errors of mean (s.e.m.) were calculated using IC₅₀/ EC₅₀/ CC₅₀ values determined in individual technical replicate experiments. To calculate IC₅₀/ EC₅₀/ CC₅₀ values, measured dose response values were fitted with 4-parameter logistic function $y = A + (B - A) / (1 + (x/C)^D)$ (model 201, XLfit, IDBS), where x refers to compound concentration and y corresponds to an assay readout value.

Leishmania donovani axenic amastigote growth inhibition assay. RPMI 1640 medium (HyClone) was supplemented with 20% heat-inactivated fetal bovine serum (Omega Scientific), 23 μM folic acid (Sigma-Aldrich), 100 μM adenosine (Sigma-Aldrich), 22 mM D-glucose (Sigma-Aldrich), 4 mM L-glutamine (Hyclone), 25 mM 2-(4-morpholino) ethanesulfonic acid (Sigma-Aldrich) and 100 IU penicillin/ 100 μg/mL streptomycin (Hyclone), and adjusted to pH = 5.5 with 6 M hydrochloric acid (Fisher Scientific) at 37 °C. *Leishmania donovani* MHOM/SD/62/1S-CL2D axenic amastigotes were cultured in 10 mL of this medium (Axenic Amastigote Medium) in T75 CELL-STAR flasks (Greiner Bio-One) at 37 °C/ 5% CO₂ and passaged once a week.

To determine compound growth inhibitory potency on *L. donovani* axenic amastigotes, 100 nL of serially diluted compounds in DMSO were transferred to the wells of white, solid bottom 384-well plates (Greiner Bio-One) by Echo 555 acoustic liquid handling system (Labcyte). Then, 1 × 10³ of *L. donovani* axenic amastigotes in 40 μL of Axenic Amastigote Medium were added to each well, and plates were incubated for 48 hours at 37 °C/ 5% CO₂. Parasite numbers in individual plate wells were determined through quantification of intracellular ATP. The CellTiter-Glo luminescent cell viability reagent (Promega) was added to plate wells, and ATP-dependent luminescence signal was measured on an EnVision MultiLabel Plate Reader (Perkin Elmer). Luminescence values in wells with compounds were divided by the average luminescence value of the plate DMSO controls, and used for calculation of compound EC₅₀ values as described above.

Axenic amastigote EC₅₀ values shown in Fig. 4b correspond to means of 2 technical replicates.

Isolation and maintenance of Leishmania donovani splenic amastigotes. Female BALB/c mice (Envigo) infected with *L. donovani* MHOM/ET/67/HU3 (ATCC) for 50–80 days were euthanized, and infected spleens were removed and weighed. The weight of an infected spleen ranged from 300 to 600 mg. For comparison, spleens from non-infected age-matched BALB/c mice weighed ~100 mg. Infected spleens were washed in Axenic Amastigote Medium (composition described above) and placed into Falcon 50 mL conical centrifuge tubes (Fisher Scientific) containing ice-cold Axenic Amastigote Medium (15 mL per infected spleen). Spleens were homogenized on ice in a Dounce homogenizer and centrifuged at 200 × g for 15 minutes at 4 °C to remove tissue debris. *Leishmania donovani* amastigotes present in the supernatant were pelleted by centrifugation at 1,750 × g for 15 min at 4 °C and re-suspended either in Axenic Amastigote Medium (when used for *in vitro* macrophage infections) or in Hanks' Balanced Salt Solution (when used for mouse infections; Hyclone). Suspensions of splenic amastigotes were kept on ice and used for *in vitro* or *in vivo* infections within 2–3 hours. To propagate *L. donovani* amastigotes *in vivo*, 6 to 7 weeks old female BALB/c mice were infected with 8 × 10⁷ purified splenic amastigotes in 200 μL of Hanks' Balanced Salt Solution by tail vein injection.

Leishmania donovani intra-macrophage amastigote growth inhibition assay. *In vitro* compound potencies on intra-macrophage *L. donovani* MHOM/ET/67/HU3 were determined using primary murine peritoneal macrophages infected with *L. donovani* splenic amastigotes. Primary macrophages were elicited in female BALB/c mice for 72 hours following the injection of 500 μL of sterile aqueous 2% starch (J. T. Baker) solution into the mouse peritoneal cavity. The protocol used for isolation of peritoneal macrophages was described in detail previously³¹. The isolated macrophages were re-suspended in Macrophage Infection Medium (RPMI-1640 medium supplemented with 2 mM L-glutamine, 10% heat-inactivated fetal bovine serum, 10 mM sodium pyruvate (Hyclone), and 100 IU penicillin/ 100 μg/mL streptomycin), and 50 μL of macrophage suspension (8 × 10⁵ macrophages/mL) were added to microscopy-grade, clear-bottom, black 384-well plates (Greiner Bio-One). Following overnight incubation at 37 °C/ 5% CO₂, plate wells were washed with Macrophage Infection Medium to remove non-adherent cells using ELx405

Select microplate washer (BioTek), and then filled with 40 μL of Macrophage Infection Medium. *Leishmania donovani* HU3 splenic amastigotes isolated from infected spleens were re-suspended in Macrophage Infection Medium at a concentration of 6 × 10⁷ cells/mL, and 10 μL of the suspension were added to assay plate wells containing adherent macrophages. After a 24-hour infection period at 37 °C/ 5% CO₂, plate wells were washed with Macrophage Infection Medium to remove residual extracellular parasites and re-filled with 50 μL of the medium. *Leishmania donovani*-infected macrophages were subsequently treated with DMSO-dissolved compounds (0.5% final DMSO concentration in the assay medium) in dose response for 120 hours at 37 °C/ 5% CO₂. Next, treated macrophages were washed with the phosphate-buffered saline buffer (PBS; Sigma-Aldrich) supplemented with 0.5 mM magnesium chloride (Sigma-Aldrich) and 0.5 mM calcium chloride (Sigma-Aldrich), fixed with 0.4% paraformaldehyde (Sigma-Aldrich) in PBS, permeabilized with 0.1% Triton X-100 (Sigma-Aldrich) in PBS, and stained with SYBR Green I nucleic acid stain (Invitrogen, 1:100,000 dilution in PBS) overnight at 4 °C. Image collection and enumeration of macrophage cells and intracellular *L. donovani* amastigotes was performed using the OPERA QEHS automated confocal microscope system equipped with 20x water immersion objective (Evotec Technologies) and the OPERA Acapella software (Evotec Technologies) as described previously³².

All reported intra-macrophage *L. donovani* EC₅₀ values were calculated from at least 3 technical replicates (n = 3 or n = 4; specified in relevant Figure captions).

Trypanosoma brucei growth inhibition assay. Bloodstream form *Trypanosoma brucei* Lister 427 parasites were continuously passaged in HMI-9 medium formulated from IMDM medium (Invitrogen), 10% heat-inactivated fetal bovine serum, 10% Serum Plus medium supplement (SAFC Biosciences), 1 mM hypoxanthine (Sigma-Aldrich), 50 μM bathocuproine disulfonic acid (Sigma-Aldrich), 1.5 mM cysteine (Sigma-Aldrich), 1 mM pyruvic acid (Sigma-Aldrich), 39 μg/mL thymidine (Sigma-Aldrich), and 14 μL/L beta-mercaptopethanol (Sigma-Aldrich); all concentrations of added components refer to those in complete HMI-9 medium. The parasites were cultured in 10 mL of HMI-9 medium in T75 CELL-STAR tissue culture flasks at 37 °C/ 5% CO₂.

To determine compound growth inhibitory potency on *T. brucei* bloodstream form parasites, 100 nL of serially diluted compounds in DMSO were transferred to the wells of white, solid bottom 384-well plates (Greiner Bio-One) by Echo 555 acoustic liquid handling system. Then, 5 × 10³ of *T. brucei* parasites in 40 μL of HMI-9 medium were added to each well, and the plates were incubated for 48 hours at 37 °C/ 5% CO₂. Parasite numbers in individual plate wells were determined through quantification of intracellular ATP amount. The CellTiter-Glo luminescent cell viability reagent was added to plate wells, and ATP-dependent luminescence signal was measured on an EnVision MultiLabel Plate Reader. Luminescence values in wells with compounds were divided by the average luminescence value of the plate DMSO controls, and used for calculation of compound EC₅₀ values as described above.

Trypanosoma brucei EC₅₀ values shown in Fig. 1 and Extended Data Fig. 3 correspond to means of 4 technical replicates.

Trypanosoma cruzi amastigote growth inhibition assay. NIH 3T3 fibroblast cells (ATCC) were maintained in RPMI 1640 medium (Life Technologies) supplemented with 10% heat-inactivated fetal bovine serum and 100 IU penicillin/ 100 μg/mL streptomycin at 37 °C/ 5% CO₂. *Trypanosoma cruzi* Tulahuen parasites constitutively expressing *Escherichia coli* beta-galactosidase³³ were maintained in tissue culture as an infection in NIH 3T3 fibroblast cells. Briefly, 2 × 10⁷ *T. cruzi* trypanomastigotes were used to infect 6 × 10⁵ NIH 3T3 cells growing in T75 CELL-STAR tissue culture flasks and cultured at 37 °C/ 5% CO₂ until proliferating intracellular parasites lysed host 3T3 cells and were released into the culture medium (typically 6–7 days). During the infection, the tissue culture medium was changed every two days. Number of *T. cruzi* trypanomastigotes present in one mL of medium was determined using a hemocytometer.

To determine compound potency on intracellular *T. cruzi* amastigotes, NIH 3T3 cells were re-suspended in phenol red-free RPMI 1640 medium containing 3% heat-inactivated fetal bovine serum and 100 IU penicillin/ 100 μg/mL streptomycin, seeded at 1,000 cells/ well (40 μL) in white, clear bottom 384-well plates (Greiner Bio-One), and incubated overnight at 37 °C/ 5% CO₂. The following day, 100 nL of each compound in DMSO were transferred to individual plate wells by Echo 555 acoustic liquid handling system. After one hour incubation, 1 × 10⁶ of tissue culture-derived *T. cruzi* trypanomastigotes, in 10 μL of phenol red-free RPMI 1640 medium supplemented with 3% heat-inactivated fetal bovine serum and 100 IU penicillin/ 100 μg/mL streptomycin were added to each well. Plates were then incubated for 6 days at 37 °C/ 5% CO₂. Intracellular *T. cruzi* parasites were quantified by measuring the activity of parasite-expressed beta-galactosidase. Ten microliters of a chromogenic beta-galactosidase substrate solution (0.6 mM chlorophenol red-β-D-galactopyranoside/ 0.6% NP-40 in PBS; both reagents from Calbiochem) were added to each well and incubated for 2 hours at room

temperature. After incubation, absorption was measured at 570 nM on SpectraMax M2 plate reader (Molecular Devices). Measured absorbance values in wells with compounds were divided by the average absorbance value of the plate DMSO controls, and used for calculation of compound EC₅₀ values as described above.

Trypanosoma cruzi amastigote EC₅₀ values shown in Fig. 1 and Extended Data Fig. 3 correspond to means of 4 technical replicates.

Trypanosoma cruzi epimastigote proliferation assay. *Trypanosoma cruzi* CL epimastigotes were continuously passaged in LIT medium containing 9 g/L liver infusion broth (Difco), 5 g/L bacto-tryptose (Difco), 1 g/L sodium chloride, 8 g/L dibasic sodium phosphate (Sigma-Aldrich), 0.4 g/L potassium chloride (Sigma-Aldrich), 1 g/L D-glucose, 10% heat-inactivated fetal bovine serum and 10 ng/mL of hemin (Sigma-Aldrich). The medium was adjusted to pH = 7.2 with 6 M hydrochloric acid. The parasites were cultured in 10 mL of LIT medium in T75 CELLSTAR tissue culture flasks at 27°C.

To determine compound growth inhibitory potency on *T. cruzi* epimastigotes, 100 nL of serially diluted compounds in DMSO were transferred to the wells of white, solid bottom 384-well plates (Greiner Bio-One) by an Echo 555 acoustic liquid handling system. Then, 5 × 10³ of *T. cruzi* epimastigotes in 40 μL of LIT medium were added to each well, and the plates were incubated for 7 days at 27°C. Parasite numbers in individual plate wells were determined through quantification of intracellular ATP amount. The CellTiter-Glo luminescent cell viability reagent was added to plate wells, and ATP-dependent luminescence signal was measured on an EnVision MultiLabel Plate Reader. Luminescence values in wells with compounds were divided by the average luminescence value of the plate DMSO controls, and used for calculation of compound EC₅₀ values as described above.

Trypanosoma cruzi epimastigote EC₅₀ values shown in Extended Data Fig. 4 correspond to means of 3 technical replicates.

Mouse fibroblast NIH 3T3 growth inhibition assay. NIH 3T3 fibroblast cells were maintained in RPMI medium 1640 with glutamine (Life Technologies) supplemented with 5% heat-inactivated fetal bovine serum and 100 IU penicillin/100 μg/mL streptomycin (3T3 Medium) at 37°C/ 5% CO₂. NIH 3T3 fibroblast cells were purchased from ATCC. We did not perform cell line authentication and did not test the cells for mycoplasma contamination. This cell line is not listed in the database of commonly misidentified cell lines maintained by ICLAC and NCBI Biosample.

To determine compound potency, NIH 3T3 cells re-suspended in 3T3 medium were seeded at 1,000 cells/ well (50 μL) in white 384-well plates (Greiner Bio-One) and incubated overnight at 37°C/ 5% CO₂. The following day, 100 nL of each compound in DMSO were transferred to individual plate wells by Echo 555 acoustic liquid handling system and plates were incubated for five days at 37°C/ 5% CO₂. Cell numbers in individual plate wells were determined through quantification of intracellular ATP amount. The CellTiter-Glo luminescent cell viability reagent was added to plate wells, and ATP-dependent luminescence signal was measured on an EnVision MultiLabel Plate Reader. Luminescence values in wells with compounds were divided by the average luminescence value of the plate DMSO controls, and used for calculation of compound CC₅₀ values as described above.

NIH 3T3 CC₅₀ values shown in Fig. 1 and Extended Data Fig. 3 correspond to means of 4 technical replicates.

Primary macrophage cytotoxicity assay. Primary macrophage cell viability was determined on mouse peritoneal macrophages infected with *L. donovani* and was expressed as the ratio of the number of macrophage cells in wells treated with a compound to those in wells treated with DMSO. The number of macrophage cells in wells was determined by high content microscopy as described previously³².

All reported macrophage CC₅₀ values were calculated from 4 technical replicates (n = 4; also specified in Figure 1 and Extended Data Figure 3 captions).

Selection of GNF3934- and GNF8000-resistant *T. cruzi* mutants. *T. cruzi* epimastigotes cultures resistant to GNF3943 and GNF8000 were generated using a methodology described previously³². Briefly, epimastigotes were initially cultured in the presence of compound concentration equivalent to its EC₂₀ value (GNF3943 EC₂₀ = 1.5 μM and GNF8000 EC₂₀ = 0.2 μM in 0.2% DMSO) or 0.2% DMSO (control). Once a week, parasites were counted and growth rates were determined. If the parasite cultures exhibited a reduced growth rate compared to 0.2% DMSO-treated parasites, epimastigotes were cultured at the same compound concentration. Once the growth rates matched that of the control epimastigote culture (0.2% DMSO), parasites were transferred into medium containing two-fold higher compound concentration. The process was repeated until significant resistance was achieved (~10- to 20-fold increase in corresponding EC₅₀ value). The time required for generation of cultures with such a level of resistance was approximately five months. Resistant clones were isolated via cloning by limiting dilution, and two independent clones were analyzed by whole genome sequencing.

T. cruzi whole genome sequencing. Chromosomal DNA isolation from GNF3943- and GNF8000-resistant *T. cruzi* clones, whole genome sequencing and sequence analysis were performed as described previously³². Sequencing reads were aligned to the *T. cruzi* CL Brenner genome³⁴.

Generation of *T. cruzi* strains ectopically expressing proteasome beta 4 subunit variants. PSMB4 TcCLB503891.100 was amplified from *T. cruzi* CL Brenner genomic DNA using KOD Hot Start DNA Polymerase (EMD Millipore), and sense (5'-AAAGCGGCCGCATGTCGGAGACAACCATTG-3') and antisense (5'-CCATGATCTTGATGTAATATAAGGCATTGCAGCCCTGCTG-3') primers. The PSMB4^{F24L} gene was generated from the wild type PSMB4 construct by site-directed mutagenesis using mutagenic sense (5'-CAGCAGGGCTGAATGCCTTATATTACATCAAGATCATGG-3') and antisense (5'-CCATGATCTTGATGTAATATAAGGCATTGCAGCCCTGCTG-3') primers and QuikChange II Site-Directed Mutagenesis Kit (Stratagene). The sequences of the wild type and mutant PSMB4 genes were verified by sequencing and both gene versions were subcloned into the *T. cruzi* expression vector pTcIndex1 under control of a T7 promoter³⁵. *Trypanosoma cruzi* CL Brenner epimastigotes were first transfected as described previously³⁶ with the pLEW13 plasmid³⁷ harboring a tetracycline-inducible T7 RNA polymerase gene. Transfected epimastigotes were selected in medium supplemented with neomycin (G418) at 500 μg/ml, and then transfected a second time with either pTcIndex1-PSMB4^{wt} or pTcIndex1-PSMB4^{F24L} plasmid. Double transfected epimastigotes were selected in the presence of 500 μg/mL of G418 (Sigma-Aldrich) and 500 μg/mL of hygromycin (Sigma-Aldrich). Susceptibility of double transfected epimastigote cell lines to compounds was assessed using induced (+5 mg/mL of tetracycline) and non-induced parasite cultures after five days of compound treatment. Parasite viability was determined with AlamarBlue (ThermoFisher Scientific).

Reported EC₅₀ values for *T. cruzi* epimastigotes ectopically expressing PSMB4 proteins were calculated from 3 technical replicates (n = 3; also specified in the Figure 3a caption).

Generation of *T. brucei* strains ectopically expressing proteasome beta 4 subunit variants. PSMB4 (Tb927.10.4710) was amplified from *T. brucei* Lister 427 genomic DNA using PCR SuperMix High Fidelity (Invitrogen), sense (5'-GCAAGCTTATGGCAGAGACGACTATCGG-3') and antisense (5'-GCGGATCCCTAGCTTACAGATTGCACTC-3') primers. The PSMB4^{F24L} gene was generated from the wild type PSMB4 construct by site-directed mutagenesis using mutagenic sense (5'-gtcgccgggttaatgcgttatactacattaagataacagg-3'), antisense (5'-ccgttatcttaatgtatataacgcattaaaccgcagc-3') primers and QuikChange II Site-Directed Mutagenesis Kit (Stratagene). The sequences of the wild type and mutant PSMB4 genes were verified by sequencing and both gene versions were cloned into the *T. brucei* expression vector pH01034 under control of a ribosomal RNA promoter. Transfected *T. brucei* Lister 427 cells were selected in medium supplemented with puromycin at 1 μg/ml. Susceptibility of transfected *T. brucei* cell lines to compounds were assessed after 2 days of compound treatment. Parasite viability was determined with CellTiter-Glo.

Reported EC₅₀ values for *T. brucei* parasites ectopically expressing PSMB4 proteins were calculated from 3 technical replicates (n = 3; also specified in the Figure 3b caption).

Purification of parasite 20S proteasomes. *T. cruzi* CL epimastigotes, *L. donovani* MHOM/SD/62/1S-CL2D axenic amastigotes and *T. brucei* Lister 27 bloodstream form trypomastigotes were grown to log phase and harvested by centrifugation. The corresponding cell pellets were stored at -80°C until further use. Prior to purification, 10 g of cell pellets were thawed, re-suspended in lysis buffer (50 mM Tris-HCl pH = 7.5, 1 mM TCEP, 5 mM EDTA, and 10 μM E-64), and lysed by passing cell suspension three times through a needle (22 gauge) and by subsequent three freeze/thaw cycles. The lysate was first cleared of cellular debris by two centrifugation steps (15,000 × g at 4°C for 15 minutes followed by 40,000 × g at 4°C for 60 minutes) and then fractionated through ammonium sulfate precipitation. The protein fraction precipitated between 45% and 65% of ammonium sulfate saturation was re-suspended in 25 mM Tris-HCl pH = 7.5, 1 mM TCEP buffer, and dialyzed overnight at 4°C against the same buffer. Proteasomes were further purified by anion exchange chromatography (Resource Q column, GE Healthcare Life Sciences) and size exclusion chromatography (Superose 6 column, GE Healthcare Life Sciences) as described elsewhere³⁸. Active fractions from the latter purification step were pooled and used in proteasome biochemical assays.

Subunit composition analysis of purified *T. cruzi* 20S proteasome by LC/MS/MS. Purified *T. cruzi* proteasome sample was buffer-exchanged and concentrated into 100 mM trimethylamine bicarbonate-HCl pH = 8.0, 150 mM NaCl buffer using a 10 kDa molecular weight cut-off micro-concentrator (Millipore Amicon Ultra). The resulting proteasome sample (200 μL, 1 mg/ml) was mixed with 5 μL of a TMTsixplex reagent (Pierce). After 60 second incubation to label primary amines, the reaction was stopped by adding 25 μL of 5% hydroxylamine. The labeled sample was run on 4–20% Bis-Tris PAGE gel (Invitrogen) to separate polypeptides. The gel was stained with eStain 2.0 (GenScript). Stained protein bands were cut out and in-gel digested separately with elastase (Promega) and asparaginase (Roche). Peptides generated by the digestions were resolved by HPLC using a vented column setup with a 2 cm Poros 10 R2 (Life Technologies, Carlsbad, CA)

self-packed pre-column, and a PepMap Easy-Spray C18 analytical column (15 cm × 75 µm ID, Thermo Scientific). Resin-bound proteolytic fragments were eluted with 2 to 40% acetonitrile / 0.1% formic acid operated at 300 nL/min for 120 min. Spectra of eluted peptide species were determined by a column-coupled Q Exactive hybrid quadrupole orbitrap mass spectrometer (Thermo Scientific). Proteome Discoverer v1.4 software (Thermo Scientific) was used to search the *T.cruzi* genome²⁸ with identified spectra for presence of 20S proteasome subunits (Supplementary Table 7). Search parameters included fixed carbamidomethyl modification of cysteine, and variable oxidation of methionine, deamidation of asparagine, pyro-glu of N-terminal glutamine, and TMT(6-plex) modification of lysine residues.

Measuring proteasome proteolytic activities. The activity of purified parasite and human 20S proteasomes was monitored by measuring cleavage of various rhodamine-labelled fluorogenic substrates. Purified 20S proteasomes were diluted in proteasome assay buffer (25 mM Tris-HCl pH 7.5, 1 mM dithiothreitol (Sigma-Aldrich), 10 mM sodium chloride, 25 mM potassium chloride, 1 mM magnesium chloride, 0.05% (w/v) CHAPS (Sigma-Aldrich) and 0.9% DMSO) at a final concentration of 162 nM (parasite proteasomes) or 25 nM (human proteasome), and pre-incubated with compound (40 nL; 0.2% final DMSO concentration) for 1 hour. Next, the following substrates (Biosynthan GmbH) were added at 3 µM final concentration to monitor specific proteolytic activities (Suc-LLVY-Rh110-dPro: chymotrypsin-like activity; Ac-RLR-Rh110-dPro: trypsin-like activity; Ac-GPLD-Rh110-dPro: caspase-like activity). The reaction was allowed to proceed for two hours at room temperature and fluorescence as a measure of purified 20S proteasome activity was monitored using the EnVision® plate reader (excitation at 485 nm/ emission at 535 nm). Km and Ki values were calculated using GraphPad Prism (GraphPad Software) 'Non-competitive enzyme inhibition' function.

Data shown in Fig. 4a, 4c, 4d and Extended Data Table 3 represent means of 3 technical replicates ($n = 3$). Data shown in Fig. 4b and Extended Data Fig. 5 represent means of 2 technical replicates ($n = 2$).

Monitoring accumulation of ubiquitylated proteins in intact cells. Growing *T. cruzi* epimastigotes were seeded into 24-well tissue culture plate (1×10^7 cells/ per well) in LIT medium and treated for 2-12 hours with DMSO (0.2%) or various concentrations of bortezomib and GNF6702 at 27°C. Following the treatment, parasites were collected by centrifugation (3,500 g for 6 minutes) and washed twice with phosphate-buffered saline (PBS). Epimastigotes were lysed by resuspending washed cells in a buffer containing 50 mM Tris-HCl pH = 7.4, 150 mM sodium chloride, 1% CHAPS, 20 µM E-64 (Sigma-Aldrich), 10 mM EDTA (Sigma-Aldrich), 5 mM N-ethylmaleimide (Sigma-Aldrich), 1 mM phenylmethylsulfonyl fluoride (Sigma-Aldrich), 10 µg/mL leupeptin (Sigma-Aldrich), 10 µg/mL aprotinin (Sigma-Aldrich), and incubating the suspension on ice for 20 minutes. Cell lysates were cleared by centrifugation at 21,000 g for 30 min at 4°C.

For 3T3 cells, 2×10^5 cells/ well were seeded into 24-well tissue culture plates in RPMI medium 1640 supplemented with 10% heat-inactivated fetal bovine serum, and incubated overnight at 37°C to allow cells to attach. Attached cells were treated for 2 hours with DMSO (0.25%) or various concentrations of bortezomib and GNF6702. Treated cells were washed twice with PBS and then lysed by incubating cells in modified RIPA buffer (50 mM Tris-HCl pH = 7.4, 1% Triton X-100, 0.2% sodium dodecylsulfate, 1 mM EDTA, 1 mM phenylmethylsulfonyl fluoride, 5 µg/mL aprotinin, 5 µg/mL leupeptin) for 30 min at 4°C. Cell lysates were cleared by centrifugation at 21,000 g for 30 min at 4°C.

Protein concentration in cell extracts was determined with BCA assay (ThermoFisher), and 10 µg of cell extracts were loaded on NuPAGE Novex 4-12% Bis-Tris gel (Invitrogen). After electrophoresis, resolved proteins were transferred to nitrocellulose membrane. Ubiquitylated proteins were detected with polyclonal anti-ubiquitin primary antibody (Proteintech, catalogue number 10201-2-AP) and rabbit anti-mouse IgG-peroxidase antibody (Sigma-Aldrich, catalogue number A0545), and then imaged using ECL Prime Western Blotting Detection Reagent (Amersham) on Chemidoc XR+ imaging system (BioRad). Collected western blot images were quantified using Image Lab software (BioRad). Briefly, rectangles of identical size and shape were drawn around each blot lane to include inside the shape all ubiquitylated protein bands within 17 - 198 kDa molecular mass range. Next, integrated signal intensities within the rectangles (reported by the Image Lab software) were used for calculation of EC₅₀ values. Three technical replicate experiments ($n = 3$) for each different dose response experiment (GNF6702 on *T. cruzi* epimastigotes; GNF6702 on 3T3 cells; bortezomib on *T. cruzi* epimastigotes; bortezomib on 3T3 cells) were performed.

Trypanosoma cruzi proteasome modeling studies. The homology model of *T. cruzi* 20S proteasome was built using 'Prime' protein structure prediction program (Schrödinger) and X-ray structure of bovine 20S proteasome (pdb accession code 1IRU)³⁹ as the template. The model was subjected to restrained minimization to relieve inter-chain clashes. 'SiteMap' program (Schrödinger) was used to identify pockets on a protein surface suitable for small molecule binding. Flexible

ligand docking was performed using 'Glide 5.8' (Schrödinger). The grid box was centered in a middle of the identified pocket and extended by 10 Å, with outer box extending additional 20 Å. The ligand was docked using the standard precision (SP) algorithm and scored using 'GlideScore' (Schrödinger). The GNF6702 GlideScore is equal to -8.5.

Receptor, enzyme and ion channel assays. GNF6702 profiling was performed at 10 µM concentration in a selectivity panel at Eurofins (www.eurofinspannlabs.com/Catalog/AssayCatalog/AssayCatalog.aspx). Listed values % change in the assay readout relative to the DMSO control. To determine inhibition of a subset of human tyrosine kinases by GNF6702, the inhibitor was profiled on a panel of Ba/F3 cell lines expressing individual Tel-activated kinases as described previously⁴⁰. All assays were performed as single technical repeats.

Determination of GNF6702 thermodynamic solubility. The solubility of GNF6702 was assessed in a high throughput thermodynamic solubility assay as described previously⁴¹. First, 25 µL of GNF6702 DMSO solutions were transferred to individual wells of a 96-well plate. DMSO was evaporated and 250 µL of 67 mM potassium phosphate buffer pH 6.8 were added to yield projected final compound concentrations from 1 µM to 100 µM. The plate was sealed to prevent solvent loss and shaken for 24 hours at room temperature. The plate was then filtered to remove non-dissolved material. Concentration of GNF6702 in individual plate wells was determined by measuring solution UV absorbance with reference to a GNF6702 calibration curve.

Determination of GNF6702 permeability in Caco-2 assay. A 96-Multiwell Insert System (BD Biosciences) was used for the Caco-2 cell culture and permeability assay as described previously⁴². Caco-2 cells were seeded onto insert wells at a density of 1.48×10^5 cells per ml and allowed to grow for 19-23 days before assays. To measure both absorptive (apical to basolateral [A-B]) and secretory (basolateral to apical [B-A]) compound transport, a solution of GNF6702 at 10 µM concentration in 0.5% DMSO were added to donor wells. The plate was incubated at 37°C for 2 hours, with samples taken at the beginning and end of the incubation from both donor and acceptor wells. The concentration of GNF6702 was determined by LC-MS/MS.

Apparent drug permeability (Papp) was calculated using the following equation:

$$\text{Papp} = dQ/dt * 1/(A * \text{Cin})$$

where dQ/dt is the total amount of a test compound transported to the acceptor chamber per unit of time (nmol/s), A is the surface area of the transport membrane (0.0804 cm²), Cin is the initial compound concentration in the donor chamber (10 µM), and Papp is expressed as cm/s.

Determination of human CYP450 inhibition by GNF6702. Extent of inhibition of major human CYP450 isoforms 2C9, 2D6 and 3A4 by GNF6702 was determined using pooled human liver microsomes and the known specific substrates of various CYP450 isoforms: diclofenac (5 µM), bufuralol (5 µM), midazolam (5 µM), and testosterone (50 µM). Probe substrate concentrations were used at concentrations equal to their reported Km values. The CYP450 inhibition assays with probe substrates diclofenac (2C9) or midazolam (3A4) were incubated at 37°C for 5 to 10 minutes using a microsomal protein concentration of 0.05 mg/mL. Probe substrates bufuralol (2D6) and testosterone (3A4) were incubated at 37°C for 20 minutes using microsomal concentration 0.5 mg/mL. The test concentrations of GNF6702 ranged from 0.5 to 25 µM in the presence of 1% DMSO. The reactions were initiated by adding NADPH (1 mM final concentration; Sigma-Aldrich) after a 5-min pre-incubation. Incubations were terminated by the addition of 300 µL of acetonitrile to 100 µL of a sample. No significant cytochrome P450 inhibition was observed. Extent of CYP450 isoform inhibition was determined by quantifying residual concentrations of individual CYP450 substrate probes at the end of reactions by LC/MS/MS.

Determination of GNF6702 in vitro metabolic stability. The intrinsic metabolic stability of GNF6702 was determined in mouse and human liver microsomes using the compound depletion approach and LC/MS/MS quantification. The assay measured the rate and extent of metabolism of GNF6702 by measuring the disappearance of the compound. The assay determined GNF6702 *in vitro* half-life ($T^{1/2}$) and hepatic extraction ratios (ER) as described previously⁴³. GNF6702 was incubated for 30 minutes at 1.0 µM concentration in a buffer containing 1.0 mg/mL liver microsomes. Samples (50 µL) were collected at 0, 5, 15 and 30 minutes and immediately quenched by addition of 150 µL of ice-cold acetonitrile/ methanol/ water mixture (8/1/1). Quantification of GNF6702 in samples was performed by LC/MS/MS, and the *in vitro* intrinsic clearance was determined using the substrate depletion method. The intrinsic clearance, CLint was calculated using the following equation:

$$\text{CLint} = (0.693/T^{1/2}) * (V/M),$$

where $T^{1/2}$ is the *in vitro* half-life, V (µL) is the reaction volume, and M (mg) is the microsomal protein amount. Finally the hepatic extraction ratio is calculated as:

$$ER = CL_h/Q_h,$$

where CL_h = hepatic clearance, Q_h = hepatic blood flow.

CL_h was calculated using the following equation:

$$CL_h = (Q_h * fu * CL_{int}) / (Q_h + fu * CL_{int}),$$

where fu = fraction unbound to protein (assumed to be 1).

Pharmacokinetic studies. An outline of various *in vitro* and *in vivo* DMPK assays used in this study for compound profiling was summarized previously⁴⁴. The pharmacokinetic properties of GNF compounds and calculation of pharmacokinetic parameters was performed as described previously²³. Mean compound plasma concentrations were calculated from fitted functions approximating compound plasma profile throughout 8 days of dosing. Blinding was not possible in these experiments.

Bioanalysis of GNF6702 in plasma. Plasma concentration of GNF6702 was quantified using a LC/MS/MS assay. Solution of 20 ng/mL of verapamil hydrochloride (Sigma-Aldrich) in acetonitrile/methanol mixture (3/1 by volume), was used as an internal standard. Twenty microliters of plasma samples were mixed with 200 µL of internal standard solution. The samples were vortexed and then centrifuged in an Eppendorf Centrifuge 5810R (Eppendorf) at 4,000 rpm for 5 minutes at 4°C to remove precipitated plasma proteins. The supernatants (150 µL) were transferred to a 96-well plate and mixed with 150 µL H₂O. The samples (10 µL) were then injected onto a Zorbax SB-C8 analytical column (2.1 x 30 mm, 3.5 µm; Agilent Technologies) and separated using a three step gradient (1st step: 1.5 mL of 0.05% formic acid in 10% acetonitrile; 2nd step: 0.5 mL of 0.05% formic acid in 100% acetonitrile; 3rd step: 0.5 mL of 0.05% formic acid in 10% acetonitrile) at flow rate of 700 µL/min. GNF6702 and verapamil were eluted at retention time 1.19 and 1.17 minutes, respectively. The HPLC system, consisting of Agilent 1260 series binary pump (Agilent Technologies), Agilent 1260 series micro vacuum degasser (Agilent Technologies) and CTC PAL-HTC-xt analytics autosampler (LEAP Technologies) was interfaced to a SCIEX API 4000 triple quadrupole mass spectrometer (Sciex). Mass spectrometry analysis was carried out using atmospheric pressure chemical ionization (APCI) in the positive ion mode. GNF6702 (430.07 > 333.20) and verapamil (455.16 > 164.90) peak integrations were performed using AnalystTM 1.5 software (Sciex). The lower limit of quantification (LLOQ) in plasma was 1.0 ng/mL. Samples were quantified using seven calibration standards (dynamic range 1 – 5,000 ng/mL) prepared in plasma and processed as described above.

Formulation of study drugs for *in vivo* efficacy experiments. All compounds administered to mice during efficacy experiments were formulated as suspensions in distilled water containing 0.5% methylcellulose (Sigma-Aldrich) and 0.5% Tween 80 (Sigma-Aldrich). During a treatment course, each mouse received 0.2 mL of drug suspension per dose by oral gavage.

Mouse model of visceral leishmaniasis. Female BALB/c mice (Envigo; 6–8 weeks old) were infected by tail vein injection with 4×10^7 *L. donovani* MHOM/ET/67/HU3 splenic amastigotes (protocol number P11-319). Seven days after infection, animals were orally dosed for eight days with vehicle (0.5% methylcellulose/ 0.5% Tween 80, miltefosine (12 mg/kg once-daily; Sigma-Aldrich), or a GNF compound (twice-daily)). On the first day of dosing, three mice were used for collection of blood for PK determination and euthanized afterwards. On the last day of dosing, PK samples were collected from remaining five mice, which were also used for determination of compound efficacy ($n = 5$ mice per group). Liver samples were collected from these five mice and *L. donovani* parasite burdens were quantified by qPCR as follows. Total DNA was extracted from drug-treated mice livers using the DNeasy Blood and Tissue Kit (Qiagen). Two types of DNA were quantified in parallel using the TaqMan assay: *L. donovani* major surface glycoprotein gp63 (Ldon_GP63) and mouse GAPDH. *L. donovani* GP63 DNA was quantified with the following set of primers: TGCGGTTTATCCTCTAGCGATAT (forward), AGTCATGAAGGGCGAGATG (reverse), and TGGCAGTACTTCACGGAC (TaqMan MGB probe, 5'-FAM-labeled reporter dye, non-fluorescent quencher). Mouse GAPDH DNA was quantified with the following set of primers: GCCGCCATGTTGCAAAC (forward primer), CGAGAGGAATGAGGTTAGTCACAA (reverse primer), and ATGAATGAACCGCCGTAT (TaqMan MGB probe, 5'-FAM-labeled reporter dye, non-fluorescent quencher). Each qPCR reaction (10 µL) included 5 µL of TaqMan Gene Expression Master Mix (Life Technologies), 0.5 µL of a 20X primer/probe mix (Life Technologies), and 4.5 µL (50 ng) of total DNA extracted from liver samples. DNA amount was quantified using the Applied Biosystems 7900HT instrument. *L. donovani* parasite burden (RU: relative units) was expressed as the abundance of *L. donovani* GP63 DNA relative to the abundance of mouse GAPDH DNA.

Mouse footpad model of cutaneous leishmaniasis. *L. major* MHOM/SA/85/JISH118 metacyclic promastigotes were generated and purified by the peanut agglutinin method as described elsewhere⁴⁵. To establish the *L. major*

footpad infection, female BALB/c mice (Envigo; 6–8 weeks old; protocol number P11-319) were injected with suspension of *L. major* metacyclic promastigotes (1×10^6 parasites in 50 µL) into each hind footpad. After eight days of infection, animals were dosed with vehicle, miltefosine (30 mg/kg once-daily), or indicated regimens of GNF6702 for seven days ($n = 6$ mice per group). The progress of infection was monitored by measuring the size (length and thickness) of hind footpad swelling using digital calipers. At the end of the study, the mice were euthanized, and the footpad tissues were extracted and used for genomic DNA isolation with the DNeasy Blood and Tissue kit (Qiagen). The *L. major* footpad burden was determined by qPCR quantification of kinetoplastid minicircle DNA (forward primer: 5'-TTTTACACCTCCCCCAGTT-3'; reverse primer: 5'-CCCGTTCATATTCCCGAAA-3'; Taqman MGB probe: 5'-AGGCCAAAAATGG-3'; 5'-FAM [6-carboxyfluorescein]-labeled reporter dye, non-fluorescent quencher). The amounts of mouse chromosomal DNA in extracted samples were quantified in parallel qPCR using a glyceraldehyde-3-phosphate dehydrogenase (GAPDH) TaqMan assay as described for mouse VL model above. *L. major* burden in footpad was expressed as the ratio of kinetoplastid minicircle DNA to mouse GAPDH. P values for the between-groups differences in efficacies were calculated with a Student's paired t test with a two-tailed distribution.

Mouse model of Chagas disease. Compound efficacy in mouse model of Chagas disease was determined as described previously²³. Female C57BL/6 mice (Envigo; 6–8 weeks old; protocol number P11-316) were infected by intraperitoneal injection with 10^3 tissue culture-derived *T. cruzi* CL trypomastigotes. Starting at 35 days after infection, the animals were dosed orally once-daily with 100 mg/kg benznidazole (Sigma-Aldrich) and indicated doses of GNF6702 (1, 3, and 10 mg/kg twice-daily, $n = 8$ per group) for 20 days. Ten days following the end of drug treatment, the mice underwent four cycles of cyclophosphamide immunosuppression, each cycle lasting one week. During each immunosuppression cycle, mice were dosed by oral gavage once-daily with 200 mg/kg cyclophosphamide (suspension in 0.5% methylcellulose/ 0.5% Tween80 aqueous solution) on day 1 and day 4 of the cycle. After the fourth immunosuppression cycle, blood samples were collected from the orbital venous sinus of each mouse, mice were euthanized and heart and colon samples were collected. Samples from treated mice were used for extraction of total DNA using the High Pure PCR template preparation kit (Roche). The amounts of *T. cruzi* satellite DNA (195-bp fragment) in extracted DNA samples were quantified by real-time qPCR TaqMan assay (Life Technologies) with the following set of primers: AATTATGAATGGCGGGAGTCA (forward primer), CCAGTGTGTGAACACGCAAAC (reverse primer), and AGACACTCTTTCAATGTA (TaqMan MGB probe, 5'-FAM [6-carboxyfluorescein]-labeled reporter dye, non-fluorescent quencher). The amounts of mouse chromosomal DNA in extracted samples were quantified in parallel qPCR reactions using a GADPH (glyceraldehyde-3-phosphate dehydrogenase) TaqMan assay as described for mouse VL model above. Each qPCR mixture (10 µL) included 5 µL of TaqMan Gene Expression master mix (Life Technologies), 0.5 µL of a 20X primer/probe mix (Life Technologies), and 4.5 µL (50 ng) of total DNA extracted from blood samples. PCRs were run on the Applied Biosystems 7900HT instrument. *T. cruzi* parasitemia was expressed as the abundance of *T. cruzi* microsatellite DNA relative to the abundance of mouse GAPDH DNA.

Mouse model of stage II HAT. Female CD1 (Charles River UK; ~8 weeks old; protocol number PPL 60/4442) mice were infected by injection into the peritoneum with 3×10^4 *T. brucei* (GVR35-VSL2) bloodstream form parasites⁴⁶.

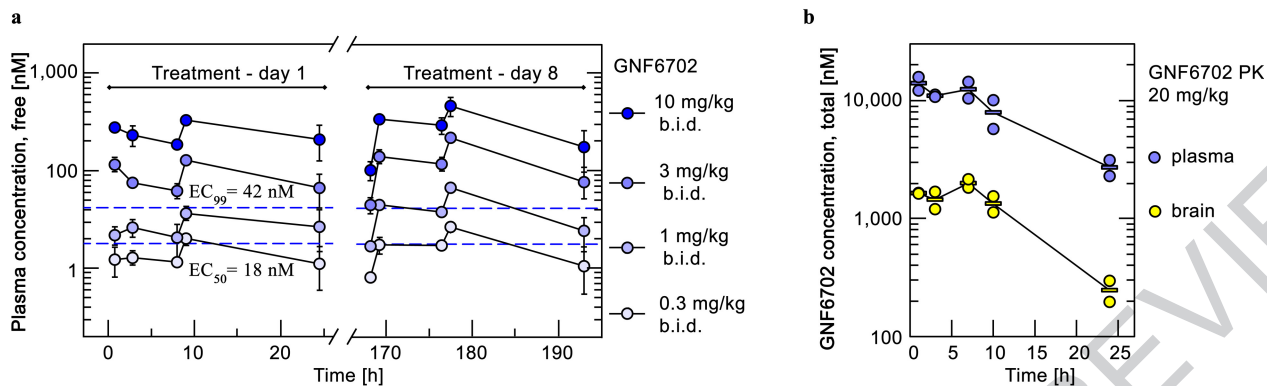
Starting on day 21, mice were dosed by oral gavage once-daily with GNF6702 ($n = 6$) at 100 mg/kg for 7 days or a single dose of diminazene acetarate (Sigma-Aldrich) at 40 mg/kg in sterile water was administered by ip injection ($n = 3$). A group of untreated mice ($n = 3$) was included as controls.

Mice were monitored weekly for parasitemia from day 21 post-infection. *T. brucei* was quantified in blood samples from the tail vein by microscopy, and *in vivo* bioluminescence imaging of infected mice was performed before treatment on day 21 post-infection and in weeks following the treatment (day 28, 35, 42, 56, 63, 72, 84, 92 post-infection). Imaging on groups of three mice was performed 10 min after ip injection of 150 mg D-luciferin (Promega)/kg body weight (in PBS) using an IVIS Spectrum (PerkinElmer) as described previously²⁵. A group of uninfected mice (aged-matched for day 0 time point; $n = 4$) were imaged using the same acquisition settings to show the background bioluminescence (Fig. 2e, grey-filled squares) in the absence of luciferase-expressing *T. brucei* after day 92 of the experiment. Untreated and diminazene-treated mice were euthanized on days 32 and 35, and day 42, respectively, due to high parasitemia or the development of symptoms related to CNS infection. GNF6702-treated mice were euthanized on day 92. No parasitemia or clinical symptoms were observed at this point. At the specified endpoints mice were sacrificed by cervical dislocation, after which whole brains were removed and imaged *ex vivo* within 10 minutes after administration of 100 µL of D-luciferin onto the brain surface. Data analysis for bioluminescence imaging was performed using Living Image Software. The same rectangular region

of interest (ROI) covering the mouse body was used for each whole body image to show the bioluminescence in total flux (photons per second) within that region. Image panels of whole mouse bodies are composites of the original images with areas outside the ROI cropped out to save space. For *ex vivo* brain images the same oval shaped ROI was used to display the bioluminescence detected for each mouse brain at the respective endpoints.

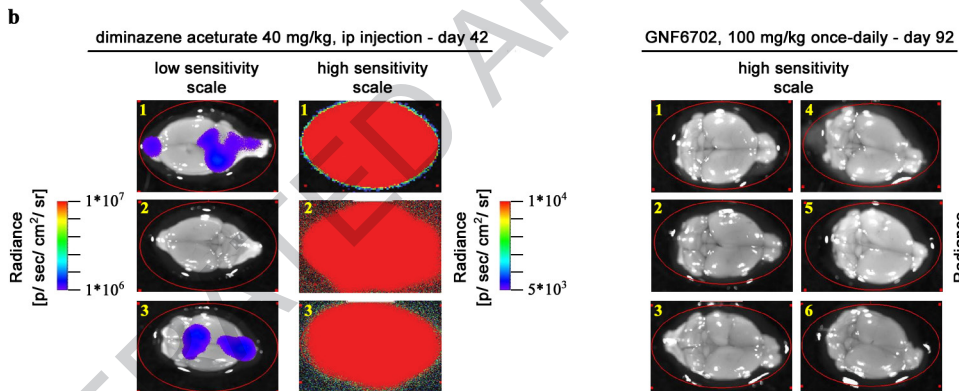
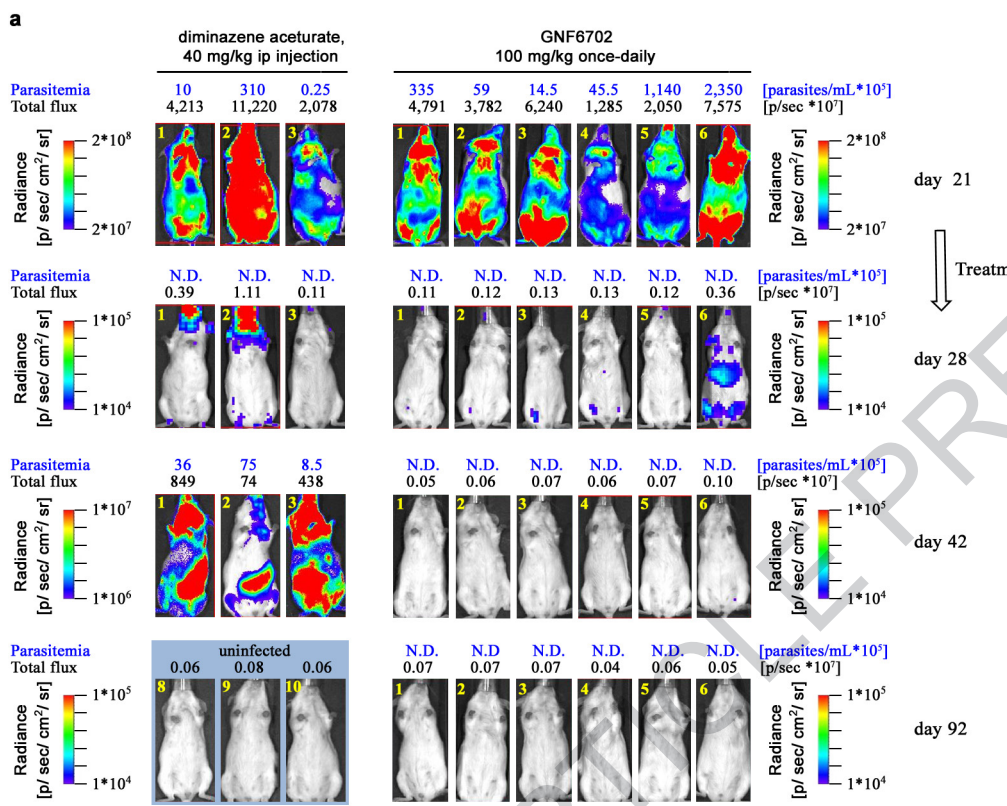
Chemical synthesis. The detailed procedures for chemical synthesis are presented in Supplementary Information.

31. Zhang, X., Goncalves, R. & Mosser, D. M. The isolation and characterization of murine macrophages. *Curr. Protoc. Immunol.* Chapter 14, Unit1 4.1 (2008).
32. Khare, S. *et al.* Utilizing chemical genomics to identify cytochrome b as a novel drug target for Chagas disease. *PLoS Pathogens* **11**, e1005058, doi:10.1371/journal.ppat.1005058 (2015).
33. Buckner, F. S., Verlinde, C. L., La Flamme, A. C. & Van Voorhis, W. C. Efficient technique for screening drugs for activity against *Trypanosoma cruzi* using parasites expressing beta-galactosidase. *Antimicrobial Agents and Chemotherapy* **40**, 2592–2597 (1996).
34. Logan-Klumpler, F. J. *et al.* GeneDB--an annotation database for pathogens. *Nucleic Acids Research* **40**, D98–108, doi:10.1093/nar/gkr1032 (2012).
35. Taylor, M. C. & Kelly, J. M. pTcINDEX: a stable tetracycline-regulated expression vector for *Trypanosoma cruzi*. *BMC Biotechnology* **6**, 32, doi:10.1186/1472-6750-6-32 (2006).
36. Hariharan, S. & Ajioka, J. & Swindle, J. Stable transformation of *Trypanosoma cruzi*: inactivation of the PUB12.5 polyubiquitin gene by targeted gene disruption. *Molecular and Biochemical Parasitology* **57**, 15–30 (1993).
37. Wirtz, E., Leal, S., Ochatt, C. & Cross, G. A. A tightly regulated inducible expression system for conditional gene knock-outs and dominant-negative genetics in *Trypanosoma brucei*. *Molecular and Biochemical Parasitology* **99**, 89–101 (1999).
38. Wilk, S. & Chen, W.-E. Purification of the eukaryotic 20S proteasome. *Curr. Protoc. Protein Sci.* Chapter 21 (2001).
39. Unno, M. *et al.* The structure of the mammalian 20S proteasome at 2.75 Å resolution. *Structure* **10**, 609–618 (2002).
40. Melnick, J. S. *et al.* An efficient rapid system for profiling the cellular activities of molecular libraries. *Proceedings of the National Academy of Sciences of the United States of America* **103**, 3153–3158, doi:10.1073/pnas.0511292103 (2006).
41. Waters, N. J., Jones, R., Williams, G. & Sohal, B. Validation of a rapid equilibrium dialysis approach for the measurement of plasma protein binding. *Journal of Pharmaceutical Sciences* **97**, 4586–4595, doi:10.1002/jps.21317 (2008).
42. Wang, J. & Skolnik, S. Recent advances in physicochemical and ADMET profiling in drug discovery. *Chemistry & Biodiversity* **6**, 1887–1899, doi:10.1002/cbdv.200900117 (2009).
43. Kalvass, J. C., Tess, D. A., Giragossian, C., Linhares, M. C. & Maurer, T. S. Influence of microsomal concentration on apparent intrinsic clearance: implications for scaling in vitro data. *Drug Metabolism and Disposition: the Biological Fate of Chemicals* **29**, 1332–1336 (2001).
44. Li, C. *et al.* A modern in vivo pharmacokinetic paradigm: combining snapshot, rapid and full PK approaches to optimize and expedite early drug discovery. *Drug Discovery Today* **18**, 71–78, doi:10.1016/j.drudis.2012.09.004 (2013).
45. Sacks, D. L. & Melby, P. C. Animal models for the analysis of immune responses to leishmaniasis. *Curr. Protoc. Immunol.* Chapter 19, Unit 19.12 (2001).
46. McLatchie, A. P. *et al.* Highly sensitive in vivo imaging of *Trypanosoma brucei* expressing "red-shifted" luciferase. *PLoS Neglected Tropical Diseases* **7**, e2571, doi:10.1371/journal.pntd.0002571 (2013).



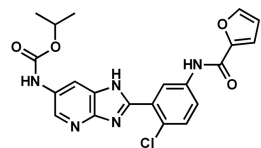
Extended Data Figure 1 | Pharmacokinetic profile of GNF6702 in mouse. **a**, Time profiles of mean free plasma concentration of GNF6702 in mouse model of visceral leishmaniasis; free GNF6702 concentration values were predicted from measured total plasma concentration values collected on day 1 and day 8 of treatment. Dashed blue lines correspond to intra-macrophage *L. donovani* EC₅₀ of 18 ± 1.8 nM and EC₉₉ of

42 ± 5.6 nM. Circles: means \pm s.d.; n = 3 mice for treatment day 1; n = 5 mice for treatment day 8; fraction unbound in mouse plasma = 0.063. For data points lacking error bars, standard deviations are smaller than circles representing means. **b**, Time course of total GNF6702 concentration in mouse plasma and brain after single oral dose (20 mg/kg); n = 2 mice per time point; circles: measured values; rectangles: means.

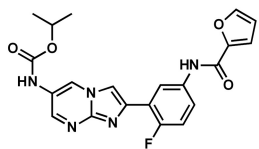


Extended Data Figure 2 | GNF6702 clears parasites from mice infected with *T. brucei*. **a,** *In vivo* quantification of bioluminescent *T. brucei* in infected mice before and after treatment. ip: intraperitoneal; day 21: start of treatment; day 28: 24 hours after last GNF6702 dose; day 42: evaluation of early parasite recrudescence in mice treated with diminazene aceturate ($n = 3$); day 42 and 92: absence of parasite recrudescence in mice treated with GNF6702 ($n = 6$). Images from uninfected mice (3 mice of 4 are shown) aged-matched for day 0 were collected independently using the same acquisition settings. Parasitemia (blue font) and whole mouse total flux (black font) values of each animal are shown above the image; N.D.: not detectable. Within each group the mouse numbers in yellow (top left in each image) refer to the same mouse imaged throughout. Complete sets of parasitemia and whole mouse total flux values collected on individual mice throughout the experiment are listed in Supplementary Tables 4 and 5. **b,** Brains from mice shown in panel a were soaked in luciferin and imaged for presence of bioluminescent *T. brucei* at the indicated time points. For three diminazene-treated mice, two images of each brain are shown, one at a lower sensitivity (left) and the other at a high signal intensity scale.

not detectable. Within each group the mouse numbers in yellow (top left in each image) refer to the same mouse imaged throughout. Complete sets of parasitemia and whole mouse total flux values collected on individual mice throughout the experiment are listed in Supplementary Tables 4 and 5. **b,** Brains from mice shown in panel a were soaked in luciferin and imaged for presence of bioluminescent *T. brucei* at the indicated time points. For three diminazene-treated mice, two images of each brain are shown, one at a lower sensitivity (left) and the other at a high signal intensity scale.

**GNF3943**

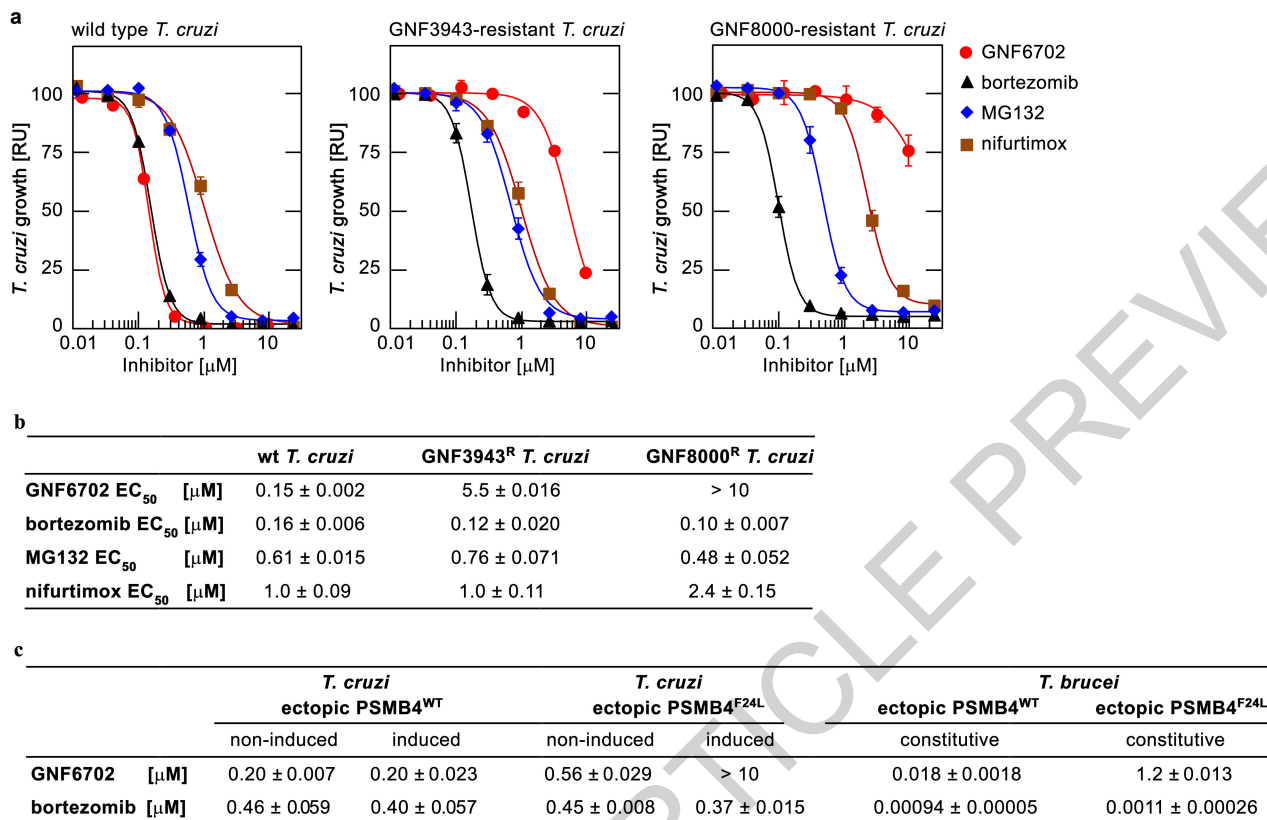
L. donovani EC₅₀ = 380 ± 23 nM
T. brucei EC₅₀ = 33 ± 9.4 nM
T. cruzi EC₅₀ = 120 ± 12 nM
 3T3 CC₅₀ = 4.5 ± 0.9 μM
 Macrophage CC₅₀ = 9.8 ± 2.4 μM
 F = 75 %
 CL = 17.7 mL·min⁻¹·kg⁻¹

**GNF8000**

L. donovani EC₅₀ = 320 ± 7.1 nM
T. brucei EC₅₀ = 73 ± 2.9 nM
T. cruzi EC₅₀ = 154 ± 12 nM
 3T3 CC₅₀ > 20 μM
 Macrophage CC₅₀ = 18 ± 2.1 μM
 F = 10 %
 CL = 8.8 mL·min⁻¹·kg⁻¹

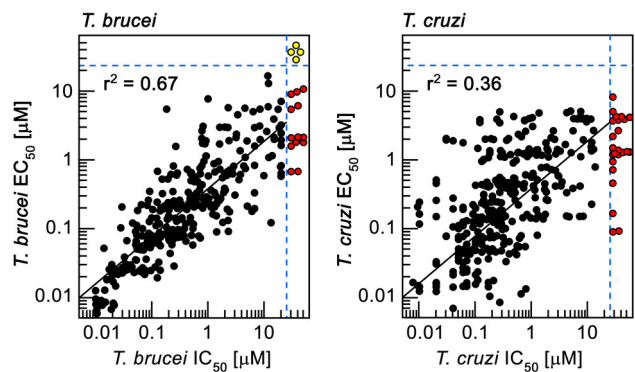
Extended Data Figure 3 | Structures and profiles of GNF3943 and GNF8000 used for selection of resistant *T. cruzi* lines. *L. donovani*: amastigotes proliferating within primary mouse macrophages; *T. brucei*: the bloodstream form tryomastigotes; *T. cruzi*: amastigotes proliferating in 3T3 fibroblast cells; macrophage: mouse primary peritoneal

macrophages; EC₅₀ and CC₅₀: half-maximum growth inhibition concentration; F: oral bioavailability in mouse after administering single compound dose (20 mg/kg) as a suspension; CL: plasma clearance in mouse after single iv bolus dose (5 mg/kg); all EC₅₀ and CC₅₀ values correspond to means ± s.e.m. (n = 4 technical replicates).

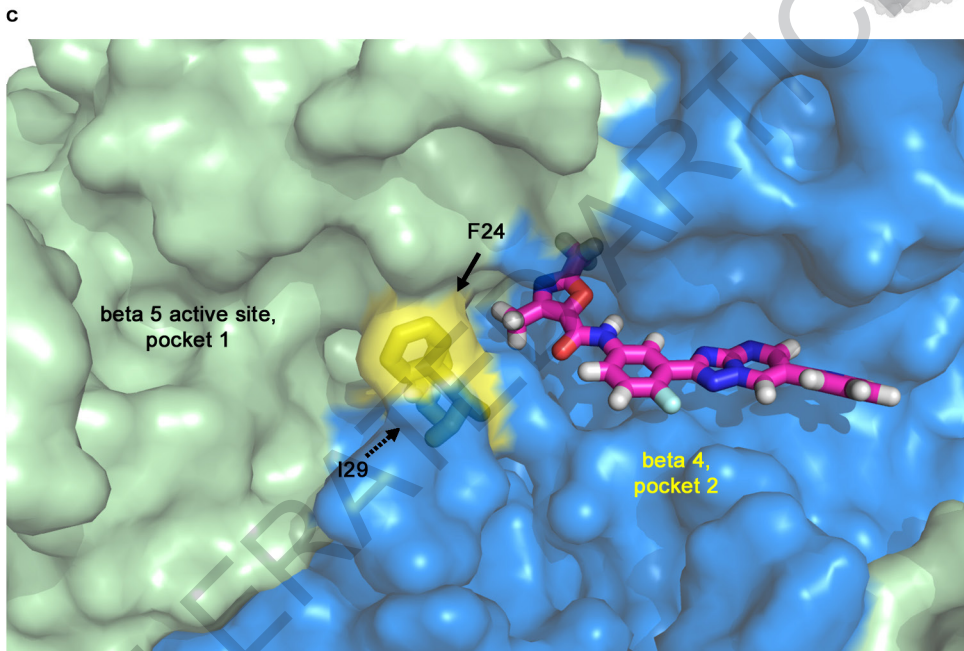
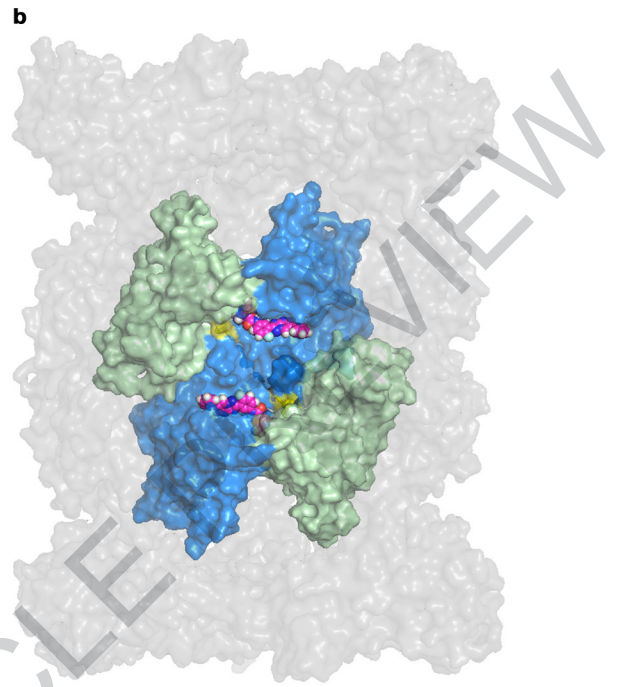
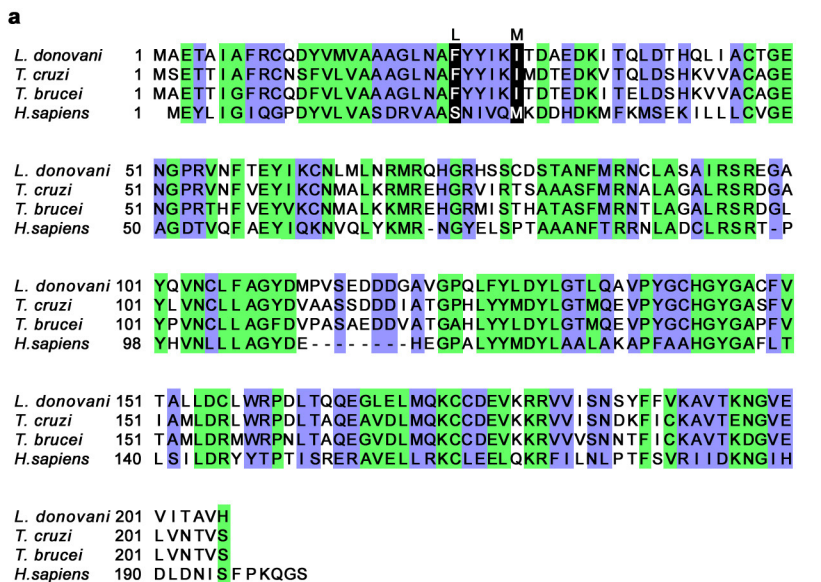


Extended Data Figure 4 | Mutations in proteasome beta 4 subunit confer resistance to GNF6702 in *T. cruzi* and *T. brucei*. **a**, growth curves of wild type, GNF3943-resistant and GNF8000-resistant *T. cruzi* epimastigote strains in the presence of increasing concentrations of GNF6702, nifurtimox, bortezomib and MG132; RU (relative units) corresponds to parasite growth relative to the DMSO control (%); for data points lacking error bars, standard errors are smaller than circles

representing means; due to limited aqueous solubility, the highest tested GNF6702 concentration was 10 μM . **b**, growth inhibition EC₅₀ values of GNF6702, bortezomib, MG132 and nifurtimox on indicated *T. cruzi* strains. **c**, growth inhibition EC₅₀ values of GNF6702 and bortezomib on *T. cruzi* epimastigotes and *T. brucei* bloodstream form trypanosomes overexpressing PSMB4^{WT} or PSMB4^{F24L}. Data shown in panels **a**, **b** and **c** correspond to means ± s.e.m. (n = 3 technical replicates).

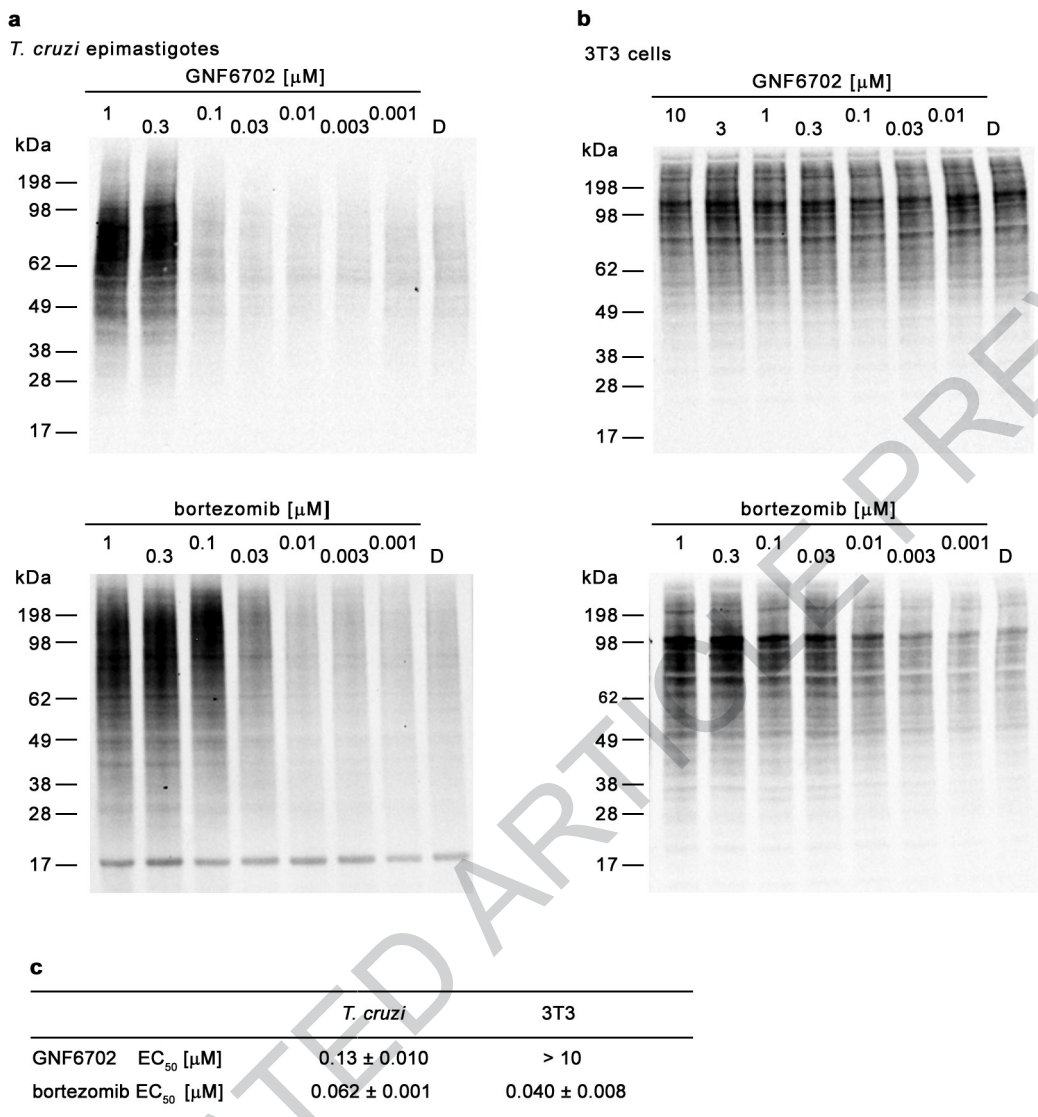


Extended Data Figure 5 | Correlation between inhibition of parasite proteasome chymotrypsin-like activity and parasite growth inhibition by the GNF6702 compound series. IC₅₀: half-maximum inhibition of indicated parasite proteasome; *T. brucei* EC₅₀: half-maximum growth inhibition on *T. brucei* bloodstream form trypanastigotes; *T. cruzi* EC₅₀: half-maximum growth inhibition on *T. cruzi* amastigotes proliferating inside 3T3 cells; data points correspond to means of 2 technical replicates; red circles: IC₅₀>20 μM; yellow circles: IC₅₀>20 μM and EC₅₀>25 μM; data for 317 analogues are shown.



Extended Data Figure 6 | Hypothetical model of GNF6702 binding to *T. cruzi* proteasome beta 4 subunit. **a**, Alignment of amino acid sequences of proteasome beta 4 subunits (PSMB4) from *L. donovani*, *T. cruzi*, *T. brucei* and *H. sapiens*. Green: amino acid residues conserved between human and kinetoplastid PSMB4 proteins; blue: amino acid residues conserved only among kinetoplastid PSMB4 proteins; black: amino acids mutated in *T. cruzi* mutants resistant to analogues from the GNF6702 series. **b**, Surface representation of the modeled *T. cruzi* 20S proteasome structure showing relative positions of the beta 5 and beta 4 subunits. Beta 4 amino acid residues F24 and I29 (colored yellow) are located at the interface of the two beta subunits. GNF6702 is depicted in a

sphere representation bound into a predicted pocket on the beta 4 subunit surface with carbon, nitrogen, oxygen and hydrogen atoms colored magenta, blue, red and grey, respectively. The other *T. cruzi* 20S proteasome subunits are colored gray. **c**, Close-up of the beta 5 and beta 4 subunits. The beta 5 subunit active site (pocket 1, chymotrypsin-like activity) is colored pale green. The predicted beta 4 pocket (pocket 2) with bound GNF6702 is colored blue. The inhibitor is shown in a stick representation with atoms colored as described in caption for the b panel. Beta 4 residues F24 and I29 are colored yellow. The proteasome model shown in panels b and c was produced by The PyMol Molecule Graphics System, Version 1.8, Schrodinger, LLC.



Extended Data Figure 7 | Effect of GNF6702 on accumulation of ubiquitylated proteins by *T. cruzi* epimastigotes and 3T3 cells.
a, Western blot analysis of *T. cruzi* whole cell extracts with anti-ubiquitin antibody after treatment with GNF6702 and bortezomib. **b**, Western blot analysis of 3T3 whole cell extracts with anti-ubiquitin antibody after treatment with GNF6702 and bortezomib. **c**, Concentrations of GNF6702 and bortezomib effecting half-maximum accumulation of ubiquitylated

proteins in *T. cruzi* and 3T3 cells (means ± s.e.m.; n = 3 technical replicates); total ubiquitin signal values in individual blot lanes shown in panels **a** and **b** were quantified and used for calculation of the listed EC₅₀ values. In **a** and **b**, numbers above the blot lanes indicate compound concentrations and D indicates control, DMSO-treated cells. For western blot source data, see Supplementary Figure 1.

Extended Data Table 1 | Point mutations identified by whole genome sequencing in GNF3943- and GNF8000-resistant *T. cruzi* epimastigotes

	Gene ID	GNF3943 ^R mutant	GNF8000 ^S mutant
Number of reads (clone 1/ clone 2)		78x10 ⁸ / 63x10 ⁸	48x10 ⁶ / 68x10 ⁸
Mapped reads (clone 1/ clone 2) [%]		87/ 87	90/ 90
Average genome coverage (clone 1/ clone 2)		82x/ 66x	51x/ 66x
Proteasome beta 4 subunit	3540409	I29M/ I29M	wt/ F24L
Dynein heavy chain	3548195	wt/ P82L	wt/ wt
Trans-sialidase	3542504	wt/ wt	wt/ G90E
Trans-sialidase	3542504	wt/ wt	wt/ L93P
Hypothetical protein TCSYLVIO_005989	3547397	wt/ wt	wt/ L627P
Hypothetical protein TCSYLVIO_005986	3547401	wt/ wt	wt/ S55P

Extended Data Table 2 | Enzyme inhibition IC₅₀ values of bortezomib and GNF6702 on three proteolytic activities of wild type *T. cruzi*, PSMB4^{I29M} *T. cruzi*, and *H. sapiens* proteasomes

		GNF6702 IC ₅₀ [μM]*	bortezomib IC ₅₀ [μM]*
wild type <i>T. cruzi</i> proteasome	chymotrypsin	0.035 ± 0.0013	0.091 ± 0.0075
	caspase	> 10	0.37 ± 0.012
	trypsin	> 10	1.7 ± 0.088
PSMB4^{I29M} <i>T. cruzi</i> proteasome	chymotrypsin	> 10	0.26 ± 0.040
	caspase	> 10	0.54 ± 0.012
	trypsin	> 10	1.6 ± 0.058
<i>H. sapiens</i> constitutive proteasome	chymotrypsin	> 10	0.030 ± 0.0070
	caspase	> 10	0.16 ± 0.007
	trypsin	> 10	7.9 ± 0.15

* mean ± s.e.m.; n= 3 technical replicates

Extended Data Table 3 | Inhibition kinetics parameters of GNF6702 on *L. donovani* and *T. cruzi* proteasomes

	chymotrypsin-like activity		caspase-like activity		trypsin-like activity	
	<i>L. donovani</i>	<i>T. cruzi</i>	<i>L. donovani</i>	<i>T. cruzi</i>	<i>L. donovani</i>	<i>T. cruzi</i>
Ki ± s.e.m. [μM]	0.055 ± 0.006*	0.079 ± 0.003*	> 10	> 10	> 10	> 10
Km ± s.e.m. [μM]	3.6 ± 0.60*	2.6 ± 0.15*	N.A.†	N.A.†	N.A.†	N.A.†
Mode of inhibition	non-competitive	non-competitive	N.A.†	N.A.†	N.A.†	N.A.†
R ² (goodness of fit)	0.91	0.97	N.A.†	N.A.†	N.A.†	N.A.†

* mean ± s.e.m.; n= 3 technical replicates

† not applicable